Acta Biomaterialia 206 (2025) 110–124

Contents lists available at ScienceDirect

Acta Biomaterialia

journal homepage: www.elsevier.com/locate/actbio

Full length article

Transient receptor potential vanilloid 4 modulates substrate stiffness mechanosensing and transcellular pore formation in human Schlemm's canal cells

Haiyan Li [a,b], Cydney Wong [a], Seyed Mohammad Siadat [a], Kristin M. Perkumas [c], Jacques A. Bertrand [d], Darryl R. Overby [d], Todd Sulchek [e], W. Daniel Stamer [c], C. Ross Ethier [a,b,e,*]

[a] Biomedical Engineering, Georgia Institute of Technology/Emory University, Atlanta, GA, United States
[b] Department of Ophthalmology, Emory University, Atlanta, GA, United States
[c] Department of Ophthalmology, Duke University, Durham, NC, United States
[d] Bioengineering, Imperial College London, London, United Kingdom
[e] Mechanical Engineering, Georgia Institute of Technology, Atlanta, GA, United States

ARTICLE INFO

Keywords:
Glaucoma
Mechanobiology
Ion channel
Calcium signaling
Tissue engineering
Hydrogel
ECM stiffening
Transcellular pore

ABSTRACT

Pathological changes in the biomechanical environment of Schlemm's canal (SC) inner wall cells, such as substrate stiffening and increased cellular stretch, are associated with ocular hypertension, a key risk factor for the development of glaucoma. Cell membrane stretch can trigger the activation of transient receptor potential vanilloid 4 (TRPV4) mechanosensitive ion channels, allowing calcium influx and initiating downstream signaling. However, the precise role of TRPV4 in SC cell mechanobiology remains unclear. Here, we demonstrate that sustained inhibition of TRPV4 activity modulates substrate stiffness mechanosensing to thereby affect the remodeling of the actin cytoskeleton and extracellular matrix of SC cells. This is accompanied by a reduction in cell stiffness and an increase in transcellular pore forming ability, potentially lowering outflow resistance and risk of ocular hypertension. Interestingly, acute activation of TRPV4 channels induces Ca^{2+} influx, increasing transcellular pore formation in SC cells. Notably, reduced TRPV4 mechanosensing is observed in glaucomatous SC cells, resulting in reduced transcellular pore forming ability. These findings suggest novel potential strategies based on targeting TRPV4 in SC cells for the treatment of ocular hypertension in glaucoma.

Statement of significance: This study identifies TRPV4 as a key mechanosensor in Schlemm's canal (SC) endothelial cells, modulating cytoskeletal dynamics, extracellular matrix remodeling, cell stiffness, and transcellular pore formation – all of which are processes central to intraocular pressure (IOP) regulation/determination. Although TRPV4 in other ocular tissues has been implicated in IOP modulation, its role in SC cell mechanobiology remained undefined. Using tissue-mimetic hydrogels and pharmacological modulation, we demonstrate that TRPV4 activity governs SC cell responses to substrate stiffness and affects transcellular pore forming ability. Notably, these mechanosensory functions are diminished in glaucomatous SC cells. Our findings underscore the complexity of SC cell mechanobiology in glaucoma and suggest that TRPV4-targeted interventions may need to be tailored to disease-specific cellular contexts.

1. Introduction

Glaucoma is the leading cause of irreversible vision loss worldwide, and elevated intraocular pressure (IOP) is the only modifiable risk factor for glaucoma [1–3]. IOP is largely determined by the resistance to aqueous humor (AH) outflow in the juxtacanalicular region of the conventional outflow pathway where the trabecular meshwork and Schlemm's canal (SC) inner wall cells interact [4]. Dysfunction in the outflow tract impairs the eye's ability to maintain IOP homeostasis, resulting in increased resistance to AH outflow and ocular hypertension

* Corresponding author at: Departments of Ophthalmology, Emory University and Biomedical Engineering, Emory/Georgia Institute of Technology, Atlanta, GA, United States.
E-mail address: ross.ethier@bme.gatech.edu (C.R. Ethier).

https://doi.org/10.1016/j.actbio.2025.09.039
Received 4 June 2025; Received in revised form 2 September 2025; Accepted 26 September 2025
Available online 27 September 2025
1742-7061/© 2025 The Authors. Published by Elsevier Inc. on behalf of Acta Materialia Inc. This is an open access article under the CC BY-NC license (http://creativecommons.org/licenses/by-nc/4.0/).

(OHT).

SC is a continuous vessel lined with endothelial cells having phenotypic characteristics of both vascular and lymphatic endothelia [5–9]. Like lymphatic vessels, cells forming the inner wall of SC experience a basal-to-apical pressure gradient that deforms these cells to create giant vacuoles and form pores that facilitate fluid drainage from the eye [10]. In primary open-angle glaucoma (POAG), the most common type of glaucoma, pathological changes in SC associated with OHT have been observed, including: a smaller lumen [11], stiffer SC inner wall cells [12,13], and decreased inner wall pore size and density [12, 14,15]. However, the mechanisms responsible for differences in responses to mechanical stimuli between normal versus glaucomatous SC inner wall cells remain unclear.

The physiological substrate of SC inner wall endothelial cells is the outermost layer of the trabecular meshwork, which is rich in extracellular matrix (ECM) and is delimited by a discontinuous basement membrane underlying the inner wall cells. In eyes with POAG, the trabecular meshwork demonstrates elevated contractility and ECM deposition, leading to tissue stiffening [13,16–20]. Consequently, SC inner wall cells in the diseased outflow tract are subject to increased biomechanical stimuli from the stiffened trabecular meshwork. In addition, these cells are continuously subjected to IOP-induced biomechanical stresses (e.g., tension, fluid shear), leading to stretching of their plasma membranes, and these effects are greater when IOP is elevated. Notably, previous studies demonstrate that SC cells in culture alter the actin remodeling of their cytoskeleton, ECM production, and cellular stiffness in response to a glaucomatous biophysical microenvironment [12,21]. It is believed that these cell-driven alterations lead to decreased outflow and consequently elevated IOP. Jointly, these pathological mechanisms can push the outflow tract to exceed its adaptive homeostatic capacity in a feed-forward loop.

Tissue health and disease are frequently governed by a complex interplay of cell-intrinsic and systemic factors, encompassing both biophysical and biochemical cues. The cellular membrane establishes a physical boundary between intracellular components and the extracellular environment, serving as a crucial interface that orchestrates responses to mechanical cues. Within cellular membranes, there resides a diverse array of mechanosensitive proteins, including integrins and mechanosensitive channels such as the transient receptor potential vanilloid 4 (TRPV4) [22–24]. TRPV4 channels are activated by mechanical stimuli such as pressure, tension, shear stress, changes in osmolarity, substrate stiffness, and pharmacological activators to allow calcium influx and thus initiate downstream signaling [24–28]. TRPV4 channels are involved in several physiological functions, such as regulating blood flow, shear stress-induced vasodilation, angiogenesis, epidermal permeability, tissue fibrosis development, and neuronal excitability [25]. Further, TRPV4 channel activity has been shown to affect functions of various ocular tissues, including the corneal epithelium, lens, ciliary body, retina, and trabecular meshwork [29–35]. Additionally, several *in vitro* and *in vivo* studies suggest that TRPV4 may play a role in glaucoma by modulating AH outflow and IOP [32,36–39], particularly through its effects on trabecular meshwork cells, or by influencing retinal ganglion cell survival [40,41]. However, the precise role of TRPV4 in SC cells remains unclear.

IOP affects the stretch of SC inner wall cells, which is expected to influence TRPV4 activity and cell function. Here we mimic IOP-induced TRPV4 activity modulation by using small molecule agonist/antagonist to explore the role of TRPV4 in regulating the function of healthy and glaucomatous human SC inner wall cells. In this manner, we investigated the potential role of TRPV4 in SC inner wall cells as a matrix stiffness sensor, influencing SC cell mechanobiology and pore forming ability.

2. Methods

2.1. SC cell isolation and culture

Primary human SC cells were isolated from ostensibly normal and glaucomatous human donor eyes, as previously described, and were cultured according to established protocols [9,42]. A total of five normal SC cell (nSC) strains isolated from healthy donor eyes and four glaucomatous cell (gSC) strains isolated from donors with a history of glaucoma were used in this study (Table 1). All SC cell strains were characterized based upon their typical spindle-like elongated cell morphology, expression of vascular endothelial-cadherin and fibulin-2, a net transendothelial electrical resistance of 10 ohms·cm^2 or greater, and lack of myocilin induction following exposure to dexamethasone. Different combinations of SC cell strains were used per experiment depending on cell availability, and all studies were conducted between cell passage 3–6. SC cells were cultured in low-glucose Dulbecco's Modified Eagle's Medium (DMEM; Gibco; Thermo Fisher Scientific) containing 10 % fetal bovine serum (FBS; HyClone, Thermo Fisher Scientific) and 1 % penicillin/streptomycin/glutamine (PSG; Gibco) and maintained at 37 °C in a humidified atmosphere with 5 % CO_2. Fresh media was supplied every 2–3 days.

2.2. Hydrogel preparation

To prepare the soft substrate, the hydrogel precursor gelatin methacryloyl (GelMA [6% w/v final concentration], Advanced BioMatrix, Carlsbad, CA, USA) was mixed with lithium phenyl-2,4,6-trimethylbenzoylphosphinate (LAP, 0.075 % w/v final concentration) photoinitiator (Sigma-Aldrich, Saint Louis, MO). Stiff substrate also incorporated methacrylate-conjugated hyaluronic acid (MA-HA; [0.25 % w/v final concentration], Advanced BioMatrix). Thirty microliters of the hydrogel solution were pipetted onto Surfasil-coated (Thermo Fisher Scientific) 18 × 18-mm square glass coverslips followed by placing 12-mm round silanized glass coverslips on top to facilitate even spreading of the polymer solution [20,21,42–44]. Hydrogels were crosslinked by exposure to UV light (CL-3000 UV Crosslinker; Analytik Jena, Germany) at 1J/cm^2. The hydrogel thickness was approximately 265 μm, calculated as the solution volume divided by the surface area of the gel on the coverslip. The hydrogel-adhered coverslips were removed with fine-tipped tweezers and placed hydrogel-side facing up in 24-well culture plates (Corning; Thermo Fisher Scientific). All the hydrogel substrates were coated with fibronectin (5 μg/cm^2; Advanced BioMatrix) at room temperature for 1 h [45].

2.3. SC cell seeding and treatments

SC cells were seeded at 2 × 10^4 cells/cm^2 on premade hydrogel substrates or glass coverslips and cultured in DMEM with 10 % FBS and

Table 1
SC cell strain information.

ID	Age	Sex	Facility (μL/min/ mm Hg)	Ophthalmic Medications
nSC74	8 months	Male	NM	N/A
nSC75	10 years	Male	NM	N/A
nSC82	56 years	Male	NM	N/A
nSC87	62 years	Male	NM	N/A
nSC89	68 years	Male	NM	N/A
gSC57	78 years	Male	NM	Unknown
gSC64	78 years	Male	0.07	Unknown
gSC90	71 years	Female	0.25	Cosopt and Latanoprost
gSC95	78 years	Male	0.1	N/A

NM = not measured. N/A = not applicable. The first letter of the ID indicates normal ("n") or glaucomatous ("g").

1 % PSG for one or two days until ~80–90 % confluence was reached. Then, SC cell-seeded hydrogels were cultured in DMEM with 10 % FBS and 1 % PSG plus the relevant activator or inhibitor, depending on the treatment protocol.

For cells grown on coverslips, the treatment paradigms were as follows: (i) control (DMSO), (ii) exposure to the TRPV4 antagonist HC067047 (HC06; 10 μM, Sigma-Aldrich) for 4 or 9 days, (iii) exposure to HC06 for 2 days followed by its removal and continued culture in control conditions for 2 or 7 days, and (iv) exposure to HC06 for 2 days followed by the removal of HC06 and addition of the TRPV4 agonist GSK1016790A (GSK101; 100 nM, Sigma-Aldrich) for 2 or 7 days.

For cells grown on hydrogels, the treatment paradigms were: (i) grown on soft substrates and treated with the TRPV4 agonist GSK101 (100 nM) for 2 days, or (ii) grown on stiff substrates and treated with the TRPV4 antagonist HC06 (10 μM) for 2 days.

2.4. Immunocytochemistry staining analysis

SC cells were fixed with 4 % paraformaldehyde (PFA; Thermo Fisher Scientific) at room temperature for 20 mins, permeabilized with 0.5 % Triton™ X-100 for 10 mins (Thermo Fisher Scientific), blocked with goat serum (BioGeneX, Fremont, CA, USA), and incubated with primary antibodies (anti-TRPV4, LS-C95181-500, 1:100, LSBio; anti-Fibronectin, ab45688, Abcam, 1:500; Cy3-anti-αSMA, C6198, Sigma-Aldrich, 1:400; anti-alpha Tubulin (acetyl K40), ab179484, Abcam, 1:1000; anti-alpha Tubulin, ab7291, Abcam, 1:1000) followed by incubation with fluorescent secondary antibody (Alexa Fluor® 488 anti-Rabbit, A27034, Invitrogen, 1:500; Alexa Fluor® 546 anti-Mouse, A11003, Invitrogen, 1:500). Nuclei were counterstained with 4′,6′-diamidino-2-phenylindole (4 μM, DAPI; Abcam, Waltham, MA, USA). Similarly, cells were stained with Phalloidin-iFluor 488 (Invitrogen; Thermo Fisher Scientific) or 594 (1:500, Cell signaling technology)/DAPI (Abcam) according to the manufacturer's instructions. Glass coverslips/hydrogel substrates were mounted with ProLong™ Gold Antifade (Invitrogen) on Superfrost™ microscope slides (Fisher Scientific), and fluorescent images were acquired with a Leica DM6 B upright microscope system or with a Zeiss LSM 700 confocal microscope system.

All fluorescent image analyses were performed using FIJI software [46] (National Institutes of Health (NIH), Bethesda, MD, USA). Fluorescence intensity of all F-actin, fibronectin (FN), or alpha smooth muscle actin (αSMA) fibers within the image was measured with image background subtraction. We then normalized the intensity by cell number and calculated fold-difference vs. control cells.

2.5. Quantitative reverse transcription-polymerase chain reaction (qRT-PCR) analysis

Total RNA was extracted from SC cells using PureLink RNA Mini Kit (Invitrogen; Thermo Fisher Scientific). RNA concentration was determined with a NanoDrop spectrophotometer (Thermo Fisher Scientific). RNA was reverse transcribed using iScript™ cDNA Synthesis Kit (Bio-Rad, Hercules, CA, USA). One hundred nanograms of cDNA were amplified in duplicates in each 40-cycle reaction using a CFX 96 Real Time PCR System (BioRad) with annealing temperature set at 60 °C, Power SYBR™ Green PCR Master Mix (Thermo Fisher Scientific), and custom-designed qRT-PCR primers (Table 2). Transcript levels were normalized to GAPDH, and mRNA fold-change calculated relative to mean control values using the comparative CT method.

Table 2
Oligonucleotide primer sequences (5′-3′) for qRT-PCR.

Target	Forward	Reverse
FN	GTCTTGTGTCCTGATCGTTG	AGGCTGGATGATGGTAGATTG
αSMA	GGCATCATCACCAACTGGGA	CAGGGTGGGATGCTCTTCAG
Collagen type I	TTTGGATGGTGCCAAGGGAG	CACCATCATTTCCACGAGCA
Collagen type IV	AATAGGTTTCCCAGGGCAGC	CAATGGCACTCCTGCAACAC
GAPDH	GTCTCCTCTGACTTCAACAGCG	ACCACCCTGTTGCTGTAGCCAA

2.6. Ca^{2+} imaging and analysis

SC cells were incubated with fluo-4AM (1 μM, Fisher Scientific) or fluo-520AM (5 μM, AAT Bioquest) in 1× HBSS solution (pH 7.4; Fisher Scientific) containing 10 mM HEPES (Fisher Scientific) for 45 min at 37 °C in a humidified atmosphere with 5 % CO_2. This was followed by a 30 min incubation with the staining buffer without the dye to remove any unloaded dye. The cells on hydrogels were then imaged using a Zeiss LSM 700 confocal microscope system.

For Ca^{2+} influx induction experiments, calcium influx was induced using the TRPV4 agonist (GSK101, 100 nM) or a combination of the TRPV4 agonist (GSK101, 100 nM) and antagonist (HC06, 10 μM). Images were captured every 5 s for 5 min, with the induction solution added after 90 s of imaging. Fluorescence intensity of intracellular Ca^{2+} was quantified using FIJI ImageJ. Cytosolic calcium increases (Ca^{2+} influx) were recorded by measuring ΔF/F (max-min), presented as relative fluorescence units.

2.7. Cell and hydrogel stiffness measurement

SC cells were seeded at 2×10^4 cells/cm^2 on premade hydrogel substrates or glass coverslips and cultured in DMEM with 10 % FBS and 1 % PSG for one or two days until cells reached ~80–90 % confluence. Then, SC cells were exposed to various conditions depending on the experiment, as described above. An MFD-3D AFM (Asylum Research, Santa Barbara, CA, USA) was used to make stiffness measurements using silicon nitride cantilevers with an attached borosilicate sphere (diameter = 10 μm; nominal spring constant = 0.1 N/m; Novascan Technologies, Inc., Ames, IA, USA). Cantilevers were calibrated by measuring the thermally induced motion of the unloaded cantilever before measurements. The trigger force was set to 600 pN to avoid substrate effects and the tip velocity was adjusted to 800 nm/s to avoid viscous effects [47]. Five measurements/cell were conducted, and at least 5 cells were measured/group of one cell strain. For hydrogel stiffness measurement, a force map covering a 20 × 20 μm area (5 × 5 grid of points) was measured. Data from AFM measurements were fitted to the Hertz model to calculate the effective Young's modulus of the cells, assuming the Poisson's ratio was 0.5.

2.8. Intracellular pore detection assay

16-well chambered glass bottom plates (Invitrogen) were plasma-treated and coated with 0.5 mg/mL biotinylated gelatin overnight at 37 °C. The gelatin was then crosslinked with microbial transglutaminase (0.1 unit/μL, Sigma-Aldrich) at 37 °C overnight. After UV sterilization of the plate, carboxyl ferromagnetic particles (4.0–4.9 μm; Spherotech Inc.) were added and incubated at room temperature for 20 min, followed by three gentle PBS washes. SC cells were seeded on top of the particles at a density of 7.5×10^3 cells/cm^2 in DMEM supplemented with 10 % FBS and 1 % PSG, and incubated for 3.5 h at 37 °C with 5 % CO_2.

To acutely activate TRPV4 channels, cells were incubated with a fluorescent tracer (Streptavidin, Alexa Fluor™ 488 Conjugate; Invitrogen) under different treatments [DMSO, 1 μM ionomycin (Sigma-Aldrich), 100 nM GSK101, and a combination of 10 μM HC06 with 100 nM GSK101] in DMEM supplemented with 10 % FBS and 1 % PSG for 2 min. The cells were then immediately washed three times with PBS, fixed with 4 % formaldehyde for 15 min at room temperature, permeabilized with 0.1 % Triton X for 15 min, and stained with Phalloidin-594 (Cell Signaling Technology) and DAPI. The glass cover was detached from the 16-well chambered system using a coverglass removal tool (Invitrogen), mounted on another glass slide with Prolong Gold Antifade Mountant (Invitrogen), and stored in the dark at 4 °C until examination

with a Leica DM6 B upright microscope system. Fluorescent and brightfield images were acquired using a 10x objective to generate tile scans for each well.

For extended TRPV4 inhibition experiments, SC cells were pretreated with 10 μM HC06 in DMEM supplemented with 10 % FBS and 1 % PSG for 2 days, followed by trypsinization and plating on particles. After 3.5 h of cell spreading, cells were incubated with the fluorescent tracer (Streptavidin, Alexa Fluor™ 488 Conjugate) under control (DMSO) or 10 μM HC06 conditions in DMEM supplemented with 10 % FBS and 1 % PSG for 5 min. The cells were then fixed, stained, and imaged as described above.

For the transcellular pore formation analysis, a 4 mm diameter circle was delineated at the center of each tile-scanned well image to exclude cells near the well edges, restricting the analysis to cells within this circle. The numbers of cells, particles beneath cells, and pores co-localized with particles were manually counted. The percentage of particle-induced pores was quantified as the number of pores associated with particles divided by the number of particles, multiplied by 100

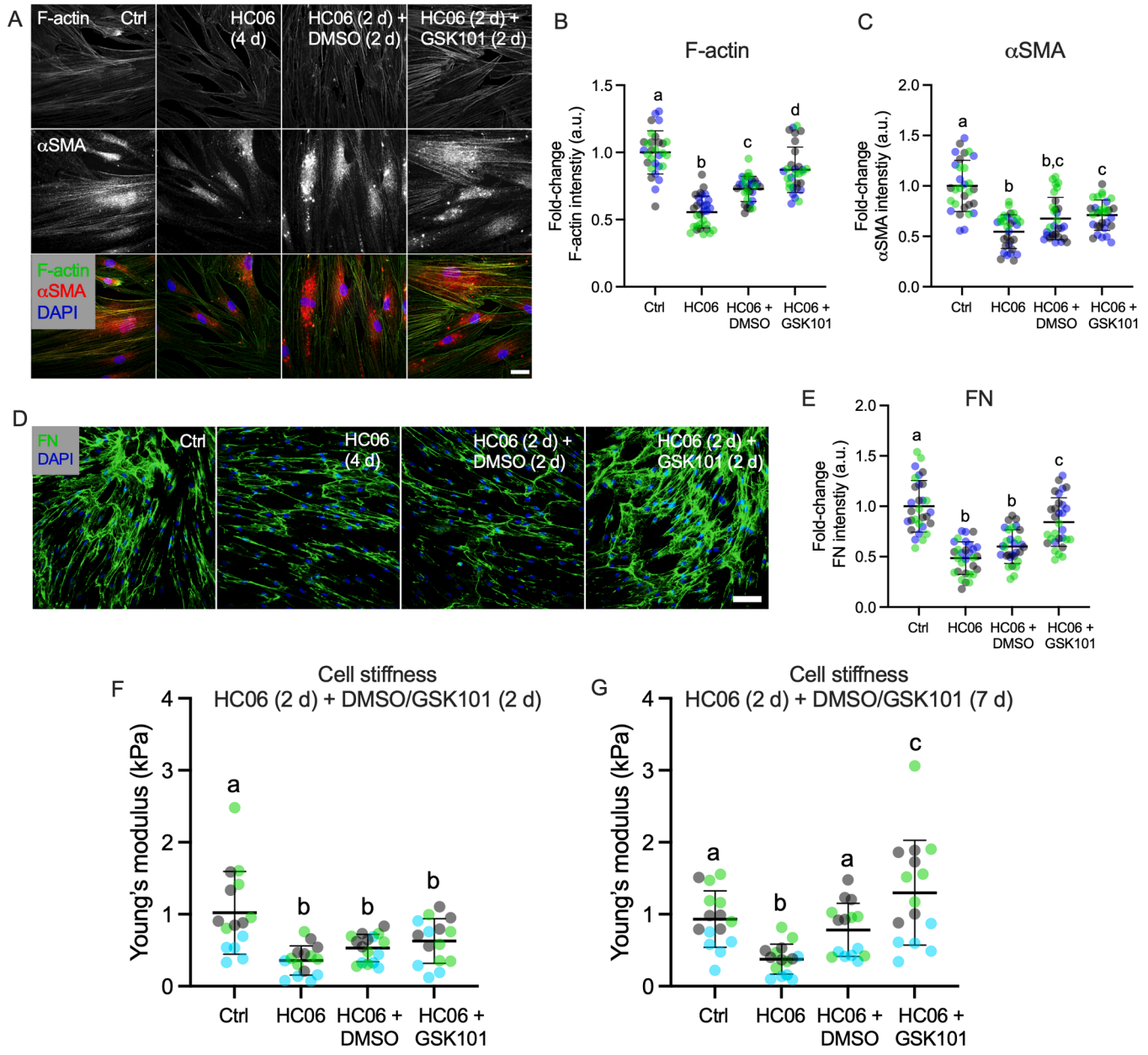


Fig. 1. TRPV4-mediated mechanobiological responses in normal Schlemm's canal (nSC) cells. (A) Representative fluorescence micrographs of F-actin and αSMA in nSC cells under the following conditions: control (DMSO); exposure to the TRPV4 antagonist HC06 (10 μM) for 4 days; exposure to the TRPV4 antagonist HC06 (10 μM) for 2 days, followed by removal of HC06 and exposure to vehicle (DMSO) for 2 days; and exposure to the TRPV4 inhibitor HC06 (10 μM) for 2 days followed by removal of HC06 and exposure to the TRPV4 agonist GSK101 (100 nM) for 2 days. Scale bar, 20 μm. **(B, C)** Plots of F-actin and αSMA normalized protein labelling intensity ($n = 30$ images per group from 3 nSC cell strains with three replicates per cell strain). **(D)** Representative fluorescence micrographs showing fibronectin (FN) expression and deposition by nSC cells. Scale bar, 100 μm. **(E)** Analysis of FN protein labelling intensity ($n = 30$ images per group from 3 nSC cell strains with three replicates per cell strain). **(F)** Young's modulus of nSC cells measured by AFM, with groups as in panel A ($n = 15$ cells per group from 3 nSC cell strains). **(G)** Young's modulus of nSC cells with groups as in panel A, except that exposure to DMSO or GSK101 was for 7 days instead of 2 days ($n = 15$ cells per group from 3 nSC cell strains). Symbols with the same colors are from the same cell strains. Lines and error bars indicate mean ± SD. Significance was determined by two-way ANOVA using multiple comparisons tests [shared significance indicator letters represent non-significant difference ($p > 0.05$), distinct letters represent significant difference ($p < 0.05$)].

[48].

2.9. Statistical analysis

Statistical analysis was conducted using GraphPad Prism, with significance set at $p < 0.05$. Sample sizes are specified in each figure caption. All data sets, except for AFM, were tested for normality using the Shapiro-Wilk test and were confirmed to meet the normality criteria ($p > 0.05$). The AFM data sets, which are expected to be log-normally distributed [49], were tested for log-normality using the Shapiro-Wilk test and met the relevant criteria ($p > 0.05$). Comparisons between groups were assessed by one-way or two-way analysis of variance (ANOVA) with Tukey's multiple comparisons *post hoc* tests, as appropriate.

3. Results

3.1. TRPV4 activity affects SC cell mechanobiology

To determine the potential role(s) of TRPV4 in SC cell mechanobiology, we first confirmed its expression in primary normal human SC (nSC) cells derived from healthy donors (**Suppl. Fig. 1A**). We then tested whether TRPV4 activation would induce Ca^{2+} influx by using the specific agonist GSK101. GSK101 increased peak Ca^{2+} levels and caused sustained Ca^{2+} elevations (measured at 250 s post-GSK101 application) in nSC cells. This intracellular influx was largely abolished when SC cells were co-treated with GSK101 and the TRPV4 antagonist HC06. We also observed that HC06 treatment alone had no detectable effect on intracellular Ca^{2+} levels in nSC cells within the measured timeframe (**Suppl. Fig. 1B, C**).

In mice, intraocular injection of the TRPV4 antagonist HC06 or topical application of its prodrug produces a sustained IOP reduction lasting several days [32,38,39], suggesting that TRPV4 inhibition in the outflow pathway has effects beyond the treatment period. This prolonged response may result from persistent biological changes or extended drug retention. Sustained TRPV4 modulation also has been shown to alter fluid conductivity, F-actin organization, and fibronectin expression in a model outflow system (trabecular meshwork cells cultured on an SU-8 polymer substrate) [32]. Based on these findings, we hypothesized that sustained IOP lowering may also involve SC inner wall cells. To test this, we treated nSC cells with the TRPV4 antagonist HC06. Following a 4-day treatment with HC06, we observed a significant reduction in F-actin stress fibers (44.5 %, $p < 0.0001$) in nSC cells (Fig. 1A, B) and decreased αSMA expression at both the transcript and protein levels compared to vehicle controls (Fig. 1A, C; **Suppl. Fig. 2A**). Upon removal of HC06 for 2 days, partial reversal of HC06-induced actin cytoskeletal remodeling was observed. Additionally, we observed that subsequent activation of TRPV4 by the agonist GSK101 for 2 days further enhanced actin remodeling compared to the group with HC06 removal alone, although cytoskeletal architecture did not fully return to control levels (Fig. 1A–C; **Suppl. Fig. 2A**).

We next examined how TRPV4 activity influences ECM produced by SC cells, given that ECM protein synthesis plays a key role in cell-ECM interactions and contributes to matrix stiffness. Fibronectin and collagen types I and IV have been previously detected in the basement membrane of the inner wall of SC [50]. As observed with actin, modulation of TRPV4 activity affected the amount of fibronectin, at both mRNA and protein levels. HC06 significantly reduced fibronectin expression compared to the vehicle control, while addition of GSK101 for 2 days after HC06 treatment for 2 days significantly increased fibronectin expression relative to the group in which HC06 was simply removed after 2 days (Fig. 1D, E; **Suppl. Fig. 2B**). Additionally, we demonstrated that transcript levels of collagen types I and IV were also affected by TRPV4 activity in nSC cells (**Suppl. Fig. 2C, D**). Importantly, we observed that TRPV4 activity influenced nSC cell stiffness, with inhibition of TRPV4 activity softening nSC cells, whereas activation of TRPV4 channels for 2 days after removing the inhibitor showed no significant effect on cell stiffness (Fig. 1F).

We further investigated whether a longer duration of TRPV4 activation could fully reverse the effects induced by a 2-day inhibition of TRPV4 activity. Therefore, after inhibiting TRPV4 activity for 2 days with the antagonist HC06 as above, HC06 was withdrawn from the culture media and nSC cells were allowed to recover in control media or were treated with the TRPV4 agonist GSK101 for 7 days. In the recovery experiment, we observed that actin remodeling and the production/deposition of ECM proteins (i.e., fibronectin, collagen types I and IV) returned nearly to control levels after removing HC06 for 7 days. Additionally, TRPV4 activation for 7 days after 2 days of TRPV4 inhibition significantly increased actin and ECM remodeling above baseline levels (**Suppl. Fig. 3**). Importantly, similar trends were observed for cell stiffness, with 7 days of TRPV4 channel activation significantly increasing cell stiffness compared to the group in which the TRPV4 antagonist was removed (1.30 ± 0.73 kPa vs. 0.78 ± 0.37 kPa; Fig. 1G). Notably, sustained TRPV4 inhibition with HC06 significantly decreased TRPV4 expression at the mRNA level in normal SC cells, whereas TRPV4 activation with GSK101 had no significant effect on TRPV4 mRNA levels (**Suppl. Fig. 4A**). Taken together, these results suggest that long-term activation of TRPV4 channels influences SC cell stiffness by modifying actin levels and influences ECM remodeling.

3.2. TRPV4 modulates nSC cell substrate stiffness mechanosensing

Previous studies have indicated that the normal trabecular meshwork has a stiffness of approximately 0.5–9 kPa, as measured by atomic force microscopy [13,16–18] (**Suppl. Table 1**). In contrast, the trabecular meshwork in glaucoma eyes is ~1.5–20-fold stiffer, depending on the measurement methods used and the location of measurement [13,16–18]. As a result, SC inner wall cells in the diseased outflow tract experience an altered microenvironment due to their underlying stiffened substrate. To study the interactions between substrate stiffness and TRPV4 channels in SC cells, we grew cells on fibronectin-coated, tissue-mimetic hydrogel substrates with defined elastic moduli of 2.36 kPa (soft) and 8.00 kPa (stiff), as measured by AFM. These values were selected to reflect both the physiological stiffness of normal trabecular meshwork tissue and the pathological increase observed in glaucomatous trabecular meshwork.

Consistent with previous studies [12,51], we observed that nSC cells on the stiff hydrogel substrate exhibited increased F-actin stress fibers and cell stiffness compared to cells on the soft substrate (**Suppl. Fig. 5A-C**). Intracellular calcium concentration is known to have an important role in the organization of F-actin [52,53]. Thus, we examined levels of intracellular calcium in nSC cells on both soft and stiff substrates, finding that steady-state intracellular Ca^{2+}concentration was significantly higher in cells residing on the stiff substrate vs. in cells on the soft substrate (1.33-fold, $p < 0.001$; Fig. 2A, B). Additionally, nSC cells residing on the stiff substrates exhibited elevated TRPV4 transcript levels vs. in cells on the soft substrate (1.31-fold, $p < 0.01$; **Suppl. Fig. 5D**). This suggests that increased TRPV4 levels on stiff substrates may, in part, contribute to increased intracellular Ca^{2+} levels.

To further investigate the role of TRPV4 channels in mechanosensing of substrate stiffness by nSC cells, we cultured cells on soft or stiff substrates and treated them with the TRPV4 agonist GSK101 or antagonist HC06, followed by assessing intracellular Ca^{2+}, F-actin, and cell stiffness. We observed that sustained TRPV4 activation in nSC cells residing on soft substrates significantly increased intracellular Ca^{2+} levels, leading to calcium levels comparable to those seen in cells grown on the stiff substrate (Fig. 2A, B). Conversely, sustained TRPV4 inhibition in cells residing on the stiff substrate decreased Ca^{2+} to levels comparable to those seen in cells residing on the soft substrate (Fig. 2A, B). Additionally, TRPV4 activation increased F-actin stress fibers in nSC cells grown on the soft substrate (1.85-fold, $p < 0.0001$; Fig. 2C, D) and induced cell stiffening ($p < 0.0001$; Fig. 2E), while TRPV4 inhibition in

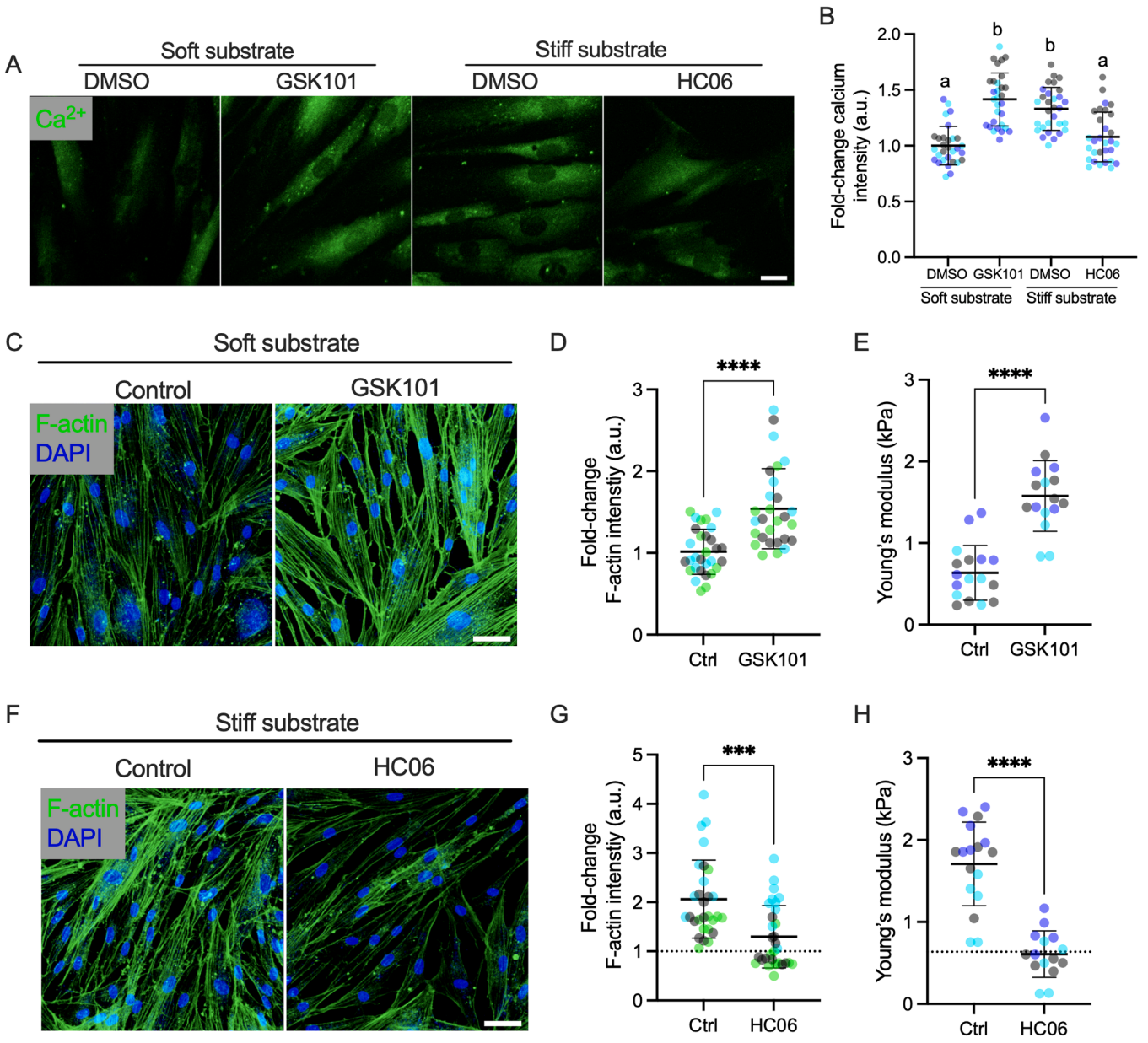


Fig. 2. TRPV4 activity in nSC cells affects their responses to substrate stiffness. (A) Representative fluorescence micrographs of intracellular Ca^{2+} in Fluo-4AM-labeled nSC cells on the soft and stiff hydrogel substrates under control (DMSO) conditions, or treated with the TRPV4 agonist GSK101 (100 nM) or antagonist HC06 (10 μM) for 2 days. Scale bars, 20 μm. **(B)** Plots of normalized intracellular Ca^{2+} fluorescence intensity ($n = 10$ images per group from 3 nSC cell strains). **(C)** Representative fluorescence micrographs of F-actin in nSC cells on the soft substrate grown for 2 days in either control (DMSO) conditions, or with the TRPV4 agonist GSK101 (100 nM) added to the media. Scale bar, 20 μm. **(D, E)** Plots of F-actin fluorescent intensity and Young's modulus measured by AFM in nSC cells exposed to control media or the TRPV4 agonist GSK101 for 2 days (100 nM; F-actin: $n = 30$ images per group from 3 nSC cell strains with three replicates per cell strain; AFM: $n = 16$–17 cells per group from 3 nSC cell strains). **(F)** Representative fluorescence micrographs of F-actin in nSC cells grown on the stiff substrate for 2 days in either control (DMSO) conditions, or with the TRPV4 antagonist HC06 (10 μM) added to the media. Scale bar, 20 μm. **(G, H)** Similar to panels (D, E), except that cell were grown on the stiff substrate and treated with a TRPV4 antagonist for 2 days. Symbols with the same colors are from the same cell strains. The lines and error bars indicate mean ± SD; dotted lines show the control mean values obtained from nSC cell grown on the soft substrate, for reference. Significance was determined by two-way ANOVA using multiple comparisons tests [shared significance indicator letters represent non-significant difference ($p > 0.05$), distinct letters represent significant difference ($p < 0.05$), ***$p < 0.001$, ****$p < 0.0001$].

cells grown on the stiff substrate reduced F-actin levels (0.60-fold, $p < 0.0001$; Fig. 2E, F) and cell stiffness ($p < 0.0001$; Fig. 2H), bringing them to levels comparable to those observed in nSC cells on the soft hydrogels. Interestingly, TRPV4 inhibition did not alter F-actin levels in nSC cells on soft substrates, nor did TRPV4 activation affect F-actin levels on stiff substrates (**Suppl. Fig. 6**). These observations indicate that modulation of cytoskeletal dynamics in nSC cells by TRPV4 is only effective over a finite range of TRPV4 activity levels, and that this range is substrate stiffness-dependent, with both subthreshold and supramaximal activity producing minimal additional effects. Taken together, these observations show that decreased levels of intracellular Ca^{2+} caused by sustained TRPV4 inhibition shift nSC cells grown on the stiff substrate toward the phenotype observed on the soft substrate, and vice versa. These findings are consistent with the concept that TRPV4 may play a role in modulating substrate stiffness responses in nSC cells.

3.3. Glaucomatous SC cells show impaired responses to TRPV4 modulation

Previous studies have shown that glaucomatous SC (gSC) cells (derived from patients with glaucoma) are stiffer and exhibit a more fibrotic phenotype compared to cells from non-glaucomatous donors [12,54]. Here, we observed that gSC cells exhibited significantly lower TRPV4 transcript levels than nSC cells (Fig. 3A), and decreased levels of peak and sustained intracellular Ca^{2+}in response to activation by GSK101 (Fig. 3B).

We next asked how gSC cells respond to sustained modulation of TRPV4 activity. Similar to nSC cells, treatment with the TRPV4 antagonist significantly reduced TRPV4 expression at the mRNA level in gSC cells, whereas the agonist had no significant effect (**Suppl. Fig. 4B**). Consistent with our findings in nSC cells, a 4-day treatment with the TRPV4 antagonist HC06 significantly decreased actin levels in gSC cells, although the magnitude of the change was less than that seen in nSC cells. Removal of the TRPV4 antagonist HC06 after 2 days restored actin to vehicle control levels. Two days of TRPV4 channel activation with GSK101 after 2 days of inhibition with HC06 showed no significant

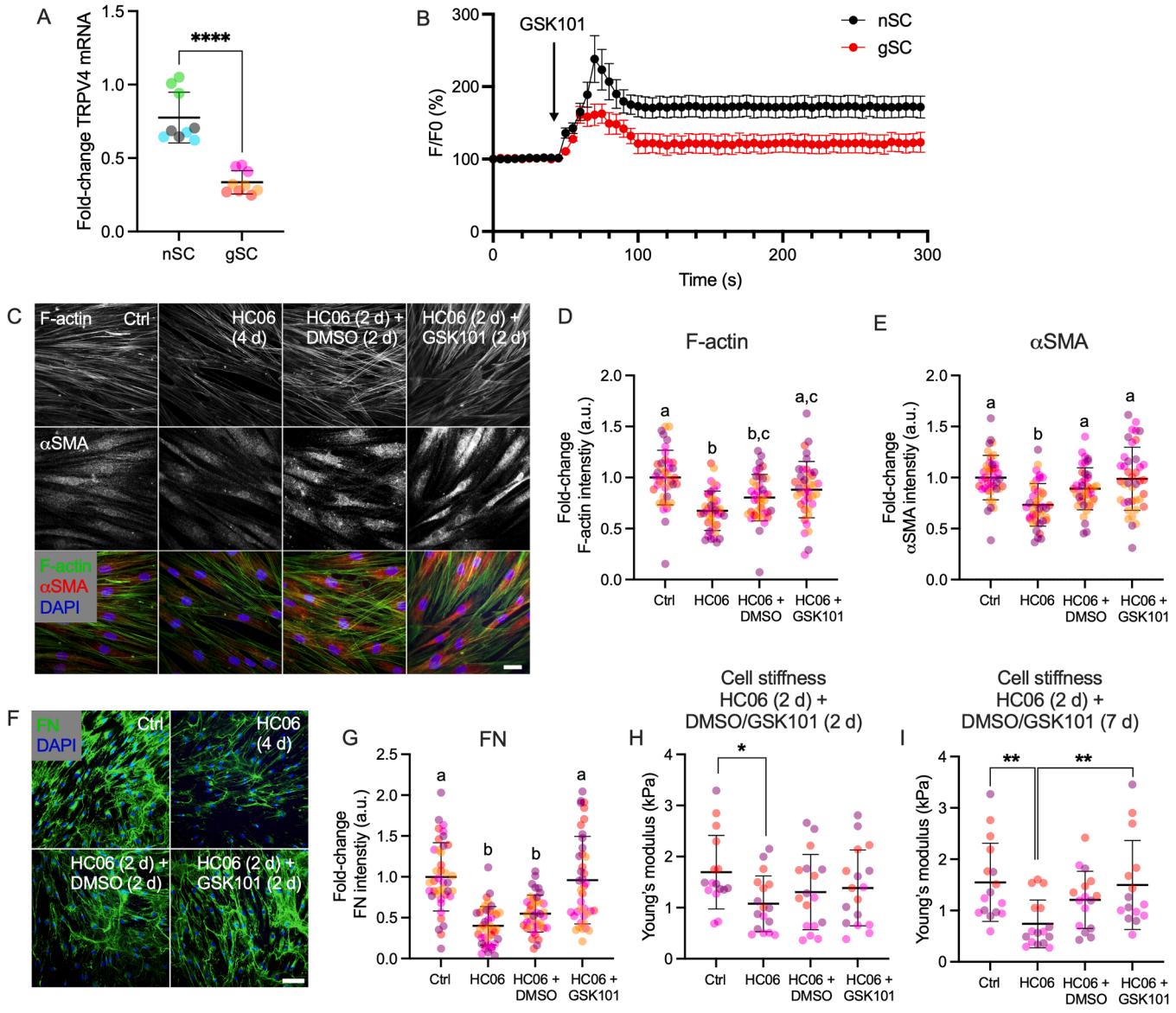


Fig. 3. Responses of glaucomatous SC (gSC) cells toTRPV4 modulation. (A) Normalized TRPV4 mRNA levels in normal (nSC) and glaucomatous (gSC) SC cells, determined by qRT-PCR (normalization to GAPDH levels; $n = 9$ replicates from 3 nSC/3 gSC cell strains). **(B)** Relative fluorescence intensities (F/F0) of the calcium indicator Fluo-4AM in nSC and gSC cells in response to the TRPV4 agonist GSK101 (100 nM; $n = 12$ replicates from 3 nSC cell strains, $n = 4$ replicates from 2 gSC cell strains). **(C)** Representative fluorescence micrographs of F-actin and αSMA in gSC cells under the following conditions: control (DMSO); exposure to the TRPV4 antagonist HC06 (10 μM) for 4 days; exposure to the TRPV4 antagonist HC06 (10 μM) for 2 days, followed by removal of HC06 and exposure to vehicle (DMSO) for 2 days; and exposure to the TRPV4 inhibitor HC06 (10 μM) for 2 days followed by removal of HC06 and exposure to the TRPV4 agonist GSK101 (100 nM) for 2 days. Scale bar, 20 μm. **(D, E)** Plots of F-actin and αSMA fluorescent labeling intensities ($n = 40$ images per group from 4 gSC cell strains with three replicates per cell strain). **(F)** Representative fluorescence micrographs of fibronectin (FN) in gSC cells cultured under various conditions as in panel A. Scale bar, 100 μm. **(G)** Plots of FN fluorescence intensity ($n = 40$ images per group from 4 gSC cell strains with three replicates per cell strain). **(H, I)** Young's modulus of gSC cells measured by AFM with either 2 (panel H; $n = 16$–17 cells per group from gSC cell strains) or 7 days treatment with TRPV4 agonist (panel I; $n = 15$–16 cells per group from 3 gSC cell strains). Symbols with the same colors are from the same cell strains. The lines and error bars indicate mean ± SD. Significance was determined by two-way ANOVA using multiple comparisons tests [$^*p < 0.05$, $^{**}p < 0.01$, shared significance indicator letters represent non-significant difference ($p > 0.05$), distinct letters represent significant difference ($p < 0.05$)].

effect on F-actin, and 7 days of activation with GSK101 significantly increased F-actin levels compared to the group with HC06 removal and DMSO addition (Fig. 3C–E; **Suppl. Fig. 7, Suppl. Fig. 8A-C**).

Interestingly, 4 days of TRPV4 channel inhibition did not affect fibronectin expression in gSC cells at the transcript level (**Suppl. Fig. 7A**), but there was a significant decrease in fibronectin expression/deposition at the protein level (Fig. 3F, G), suggesting perhaps that TRPV4 may influence proteins associated with fibronectin degradation. No significant change in fibronectin was detected with HC06 removal, and both 2 days and 7 days of TRPV4 channel activation significantly increased fibronectin at the protein level, but not at the mRNA level (Fig. 3**F, G; Suppl. Fig. 5, Suppl. Fig. 8D, E**). We also observed that TRPV4 activation in gSC cells increased the mRNA levels of collagen types I and IV, but these effects were dampened compared to those seen in nSC cells (**Suppl. Fig. 7**).

Consistent with a previous report [12], gSC cells were measured to be stiffer than nSC cells by AFM (Fig. 3H, I). Comparable to the trends observed with F-actin, both TRPV4 inhibition and activation modulated

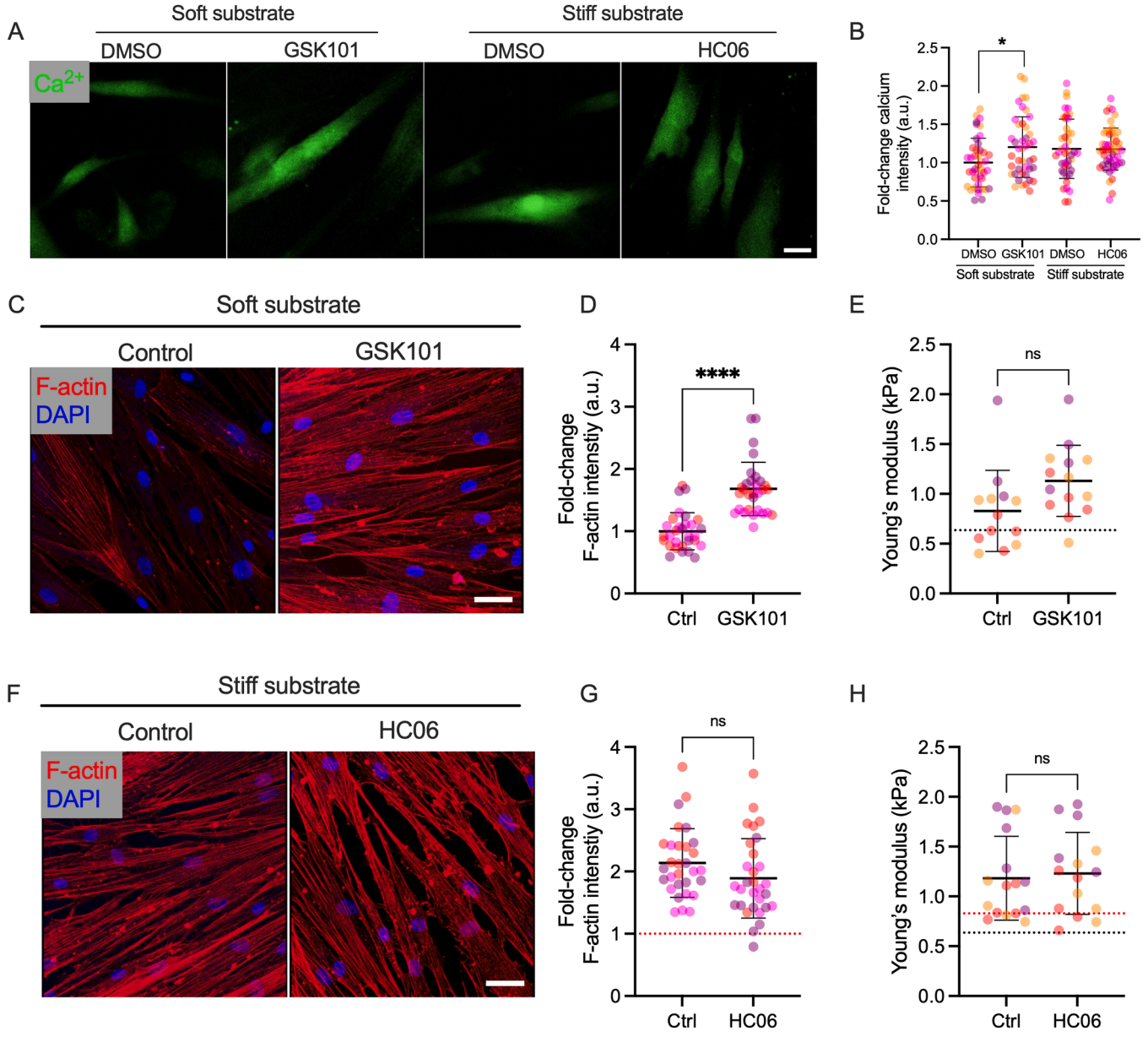


Fig. 4. Impaired TRPV4-modulated substrate stiffness mechanosensing in gSC cells. (A) Representative fluorescence imaging of intracellular Ca^{2+} in Fluo-4AM-labeled gSC cells cultured on the soft and stiff hydrogel substrates, under control conditions or after modulation of TRPV4 activity for 2 days. Scale bars, 20 μm. **(B)** Plots of normalized intracellular Ca^{2+} fluorescence intensity corresponding to conditions shown in panel A ($n = 40$ images per group from 4 gSC cell strains with three replicates per cell strain). **(C)** Representative fluorescence micrographs of F-actin in gSC cells on the soft substrate grown for 2 days in either control (DMSO) conditions, or with the TRPV4 agonist GSK101 (100 nM) added to the media. Scale bar, 20 μm. **(D, E)** Plots of F-actin fluorescent intensity and Young's modulus measured by AFM in gSC cells exposed to control media or the TRPV4 agonist GSK101 for 2 days (100 nM; F-actin: $n = 30$ images per group from 3 gSC cell strains with three replicates per cell strain; AFM: $n = 16$–17 cells per group from 3 gSC cell strains). **(F)** Representative fluorescence micrographs of F-actin in gSC cells grown on the stiff substrate for 2 days in either control (DMSO) conditions, or with TRPV4 antagonist HC06 (10 μM) added to the media. Scale bar, 20 μm. **(G, H)** Plots of F-actin fluorescent intensity and Young's modulus measured by AFM in gSC cells exposed to control media or the TRPV4 antagonist HC06 for 2 days (10 μM; F-actin: $n = 30$ images per group from 3 gSC cell strains with three replicates per cell strain; AFM: $n = 15$–17 cells per group from 3 gSC cell strains). Symbols with different colors represent different cell strains. The lines and error bars indicate Mean ± SD; black and red dotted lines show nSC and gSC cell on the soft substrate control mean value for reference. Significance was determined by two-way ANOVA using multiple comparisons tests (*$p < 0.05$, ****$p < 0.0001$).

cell stiffness to a lesser extent in gSC cells vs. in nSC cells. Specifically, 4 days of TRPV4 inhibition decreased nSC cell stiffness by 64.7 %, while it reduced gSC cell stiffness by only 36.6 %; and 7 days of TRPV4 activation increased cell stiffness by 1.58-fold in nSC cells, but only by 1.25-fold in gSC cells compared to the group with HC06 removal alone (Fig. 1F, G and Fig. 3H, I). Overall, these results demonstrate that, in contrast to normal SC cells, gSC cells exhibit an impaired response to TRPV4 modulation.

Next, we sought to investigate the interplay between TRPV4 activity and substrate stiffness mechanosensing in gSC cells. Intracellular Ca^{2+} levels showed a 1.18-fold increase on stiff versus soft substrates; however, this difference was not statistically significant. Interestingly, TRPV4 activation significantly increased intracellular Ca^{2+} levels in gSC cells on the soft substrate, while no significant difference was observed between TRPV4 antagonist-treated and control cells on the stiff substrate (Fig. 4A, B). Similar to observations in nSC cells, gSC cells exhibited higher levels of F-actin and cell stiffness on the stiff substrate compared to the soft substrate (Fig. 4C–H). Unexpectedly, sustained TRPV4 activation significantly increased F-actin, but not stiffness, in gSC cells on the soft substrate (Fig. 4C–E), while sustained TRPV4 inhibition showed no effect on either F-actin or stiffness in gSC cells on the stiff substrate (Fig. 4F–H). Similar to nSC cells, inhibition of TRPV4 channels in gSC cells on soft substrates or their activation on stiff substrates had no effect on F-actin cytoskeleton (**Suppl. Fig. 9**). Taken together, these results confirm that interactions between TRPV4 activity and the response to substrate stiffness are muted in glaucomatous SC cells as

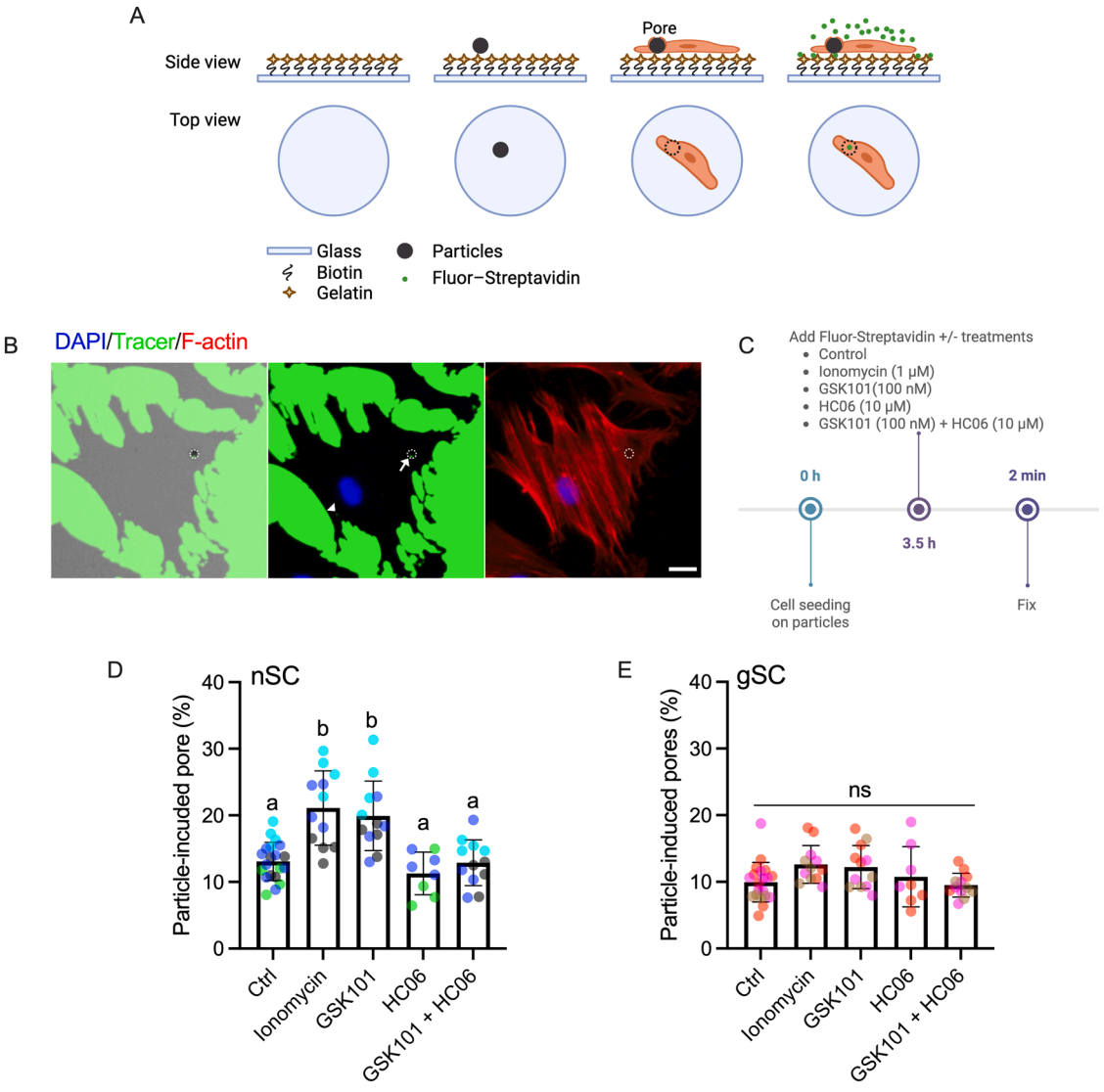


Fig. 5. Rapid TRPV4 activation induces upregulation of intracellular Ca^{2+} and enhances transcellular pore formation in SC cells. (A) Schematic showing particles for inducing, and fluorescence assay for detecting, pores in SC cells. Carboxyl particles (4.0–4.9 μm diameter) were seeded on a biotinylated gelatin substrate, followed by plating of normal or glaucomatous SC cells. Subsequently, fluorescently-tagged streptavidin was introduced into the culture media. **(B)** Representative fluorescent micrographs showing spots where fluorescently tagged streptavidin (green) has bound with biotin substrate under cultured SC cells (at sites of intracellular pores) as well as surrounding regions not covered by cells. White circles outline particles. The arrow indicates a particle-induced pore, while the arrowhead points to a spontaneously formed pore detected by the fluorescent assay but not associated with a particle. Scale bar: 50 μm. **(C)** Schematic showing the time course of pore formation assay: SC cells were seeded atop particles on a biotinylated gelatin-coated glass substrate. Three and half hours after cell seeding, fluorescently-tagged streptavidin plus the relevant treatment (DMSO [control], 1 μM ionomycin, 100 nM GSK101, 10 μM HC06, or co-treatment with 10 μM HC06 plus 100 nM GSK101) was introduced into the culture media and incubated for 2 mins. Created with BioRender.com. **(D)** Pore incidence (percentage of particles associated with pores) in nSC cells ($n = 4$ wells per nSC cell strain). **(E)** Pore incidence in gSC cells ($n = 4$ wells per gSC cell strain). Symbols with different colors represent different cell strains. The lines and error bars indicate Mean ± SD. Significance was determined by two-way ANOVA using multiple comparisons tests [shared significance indicator letters represent non-significant difference ($p > 0.05$), distinct letters represent significant difference ($p < 0.05$)].

compared to normal SC cells.

3.4. Acute TRPV4 activation increases transcellular pore formation

To drain from the eye via SC, aqueous humor passes through micron-sized pores in the inner wall of SC; further, these pores play a crucial role in modulating IOP [7,12,55]. Thus, there is great interest in understanding mechanobiological signaling processes that modulate SC cell pore formation. It is also well known that IOP can fluctuate over very short time scales, even within seconds or minutes, due to physiological events such as blinking and gaze adjustment [56,57]. IOP elevation is known to cause stretching of the plasma membranes of SC inner wall cells, which in turn is expected to activate TRPV4 mechanosensitive ion channels and promote Ca^{2+} influx. We hypothesized that acute TRPV4 activation-induced intracellular Ca^{2+} elevation could influence transcellular pore formation in SC cells, thereby modulating outflow facility and IOP. Membrane fusion is required for transcellular pore formation, and emerging evidence suggests that intracellular Ca^{2+} dynamics is a key modulator of membrane fusion and fusion-pore expansion [58].

To assess transcellular pore formation in SC cells, our lab has previously developed an *in vitro* assay that subjects SC cells to localized cellular stretching [59]. In this assay, carboxyl microspheres (4.0–4.9 μm diameter) are seeded on a biotinylated gelatin substrate, followed by plating of SC cells. Subsequently, fluorescently-tagged streptavidin is introduced into the culture media. The fluorescently-tagged streptavidin traverses the SC cell monolayer at locations where transcellular pores (or gaps between cells) exist, thereby irreversibly adhering to the biotinylated substrate and thus generating an observable persistent fluorescent signal (Fig. 5A).

Using our pore forming assay, we observed that basal-to-apical cellular stretching imparted by particles underlying SC cells caused transcellular pore formation (Fig. 5B). To investigate the acute effects of TRPV4 activation on transcellular pore formation in SC cells, GSK101 was added to the media overlying cells along with the fluorescent tracer. Ionomycin, an effective Ca^{2+} ionophore, was used as a positive control for intracellular Ca^{2+} induction (Fig. 5C). In normal cells, 13.1 % of particles exhibited an associated pore, and both ionomycin and TRPV4 activation significantly increased particle-induced pore formation, while co-treatment of HC06 with GSK101 blocked TRPV4 activation-induced transcellular pore formation. Notably, HC06 treatment alone showed no effect on SC cell transcellular pore formation, aligning with the observation that HC06 exhibited no impact on intracellular Ca^{2+} levels during short-term treatment. To further investigate whether TRPV4 activation-induced transcellular pore formation is Ca^{2+}-dependent, we treated cells with GSK101 using media either with or without Ca^{2+}. We found that GSK101 failed to induce transcellular pore formation in the absence of Ca^{2+} in the media, in contrast to the robust effect observed under Ca^{2+}-rich conditions (**Suppl. Fig. 10**). These data are consistent with the hypothesis that TRPV4 activation can promote transcellular pore formation in normal SC cells by upregulating intracellular Ca^{2+} (Fig. 5D).

In glaucomatous SC cells, 9.9 % of particles were associated with pores, which was significantly lower than the frequency observed in normal cells, consistent with previously observed differences in transcellular pore formation between normal vs. glaucomatous SC cells, both in native tissues and in an *in vitro* assay inducing transcellular pore formation by fluid flow across SC cell monolayers [12,14]. A similar pattern of TRPV4 activation and ionomycin effects on transcellular pore formation was observed in gSC cells as in nSC cells; however, the effects of TRPV4 activity modulation/intracellular Ca^{2+} elevation were attenuated in gSC cells compared to normal cells, and the differences were not statitistically significant (Fig. 5E). Specifically, in nSC cells, ionomycin and GSK101 increased transcellular pore formation rate by 1.61- and 1.52-fold compared to control conditions, respectively, whereas these increases were only 1.27- and 1.23-fold in gSC cells. Together, these results indicate that acute TRPV4 activation-induced upregulation of intracellular Ca^{2+} enhances transcellular pore formation in SC cells, with greater efficiency observed in normal cells compared to glaucomatous cells.

3.5. Extended TRPV4 inhibition promotes transcellular pore formation in nSC cells, but not in gSC cells

Previous studies have shown a strong inverse association between transcellular pore formation and cell stiffness in SC cells [12,48]. In this study, we have demonstrated that long-term inhibition of TRPV4 activity decreases SC cell stiffness. Therefore, we hypothesized that long-term inhibition of TRPV4 channels would also elevate the ability of SC cells to form transcellular pores. To test this hypothesis, SC cells were treated with HC06 in high serum conditions for two days. We used high serum for these experiments, since we observed that low serum conditions affected cell spreading time, which in turn adversely impacted the pore detection assay. After treatment, the cells were trypsinized and plated on particles to induce transcellular pore formation using the assay described above (Fig. 6A).

First, we confirmed that actin and fibronectin levels remained depressed by TRPV4 inhibition after trypsinization in both nSC and gSC cells (**Suppl. Fig. 11**). By measuring cell stiffness using AFM, and by measuring transcellular pore formation rate as described above, we also observed that inhibiting TRPV4 for two days in high serum conditions significantly decreased cell stiffness in three out of the four normal cell strains tested (Fig. 6B). The exception was nSC75 cells, in which cell stiffness was decreased from 1.50 ± 0.74 kPa to 1.18 ± 0.32 kPa, but this difference did not reach statistical significance. Using our pore forming assay, we found that transcellular pore formation rate was increased in two of the four cell strains tested, with the other strains showing a trend that did not reach statistical significance (Fig. 6C). However, despite the variability in particle-induced pore formation rates across the tested cell strains, pooled data showed that long-term TRPV4 inhibition significantly increased particle-induced pore formation in nSC cells compared to vehicle controls (20.3 ± 5.6 % vs. 12.3 ± 2.9 %; Fig. 6D).

We next repeated these experiments in gSC cells. Interestingly, no significant changes were observed in either cell stiffness or particle-induced pore formation for any of the individual gSC cell strains tested (Fig. 6E, F). Pooling the data from all cell strains revealed a small increase in transcellular pore formation rate associated with TRPV4 inhibition (10.8 ± 3.8 % vs. 9.2 ± 2.0 %); however, this difference was not statistically significant (Fig. 6G).

Sustained TRPV4 inhibition downregulated F-actin in both normal and glaucomatous cells, but this did not translate to significant changes in cell stiffness. We thus investigated whether other cytoskeletal elements that could influence SC cell stiffness, specifically microtubules (MTs) [60], were modulated by TRPV4 activity. MT stability has been shown to influence actin organization, cell contractility, and stiffness in other cell types [61–66]. Further, acetylation is a proxy for MT stability [67]; therefore, we assessed the effects of TRPV4 inhibition on MT acetylation. By analyzing the ratio of acetylated α-tubulin to total α-tubulin, we found that sustained TRPV4 inhibition significantly decreased MT stability in both normal and glaucomatous SC cells (Fig. 6H–J). This suggests that changes in MT stability, along with F-actin changes, may influence cell stiffness. Overall, these data suggest that long-term TRPV4 inhibition increases the rate of particle-induced pore formation in nSC cells by modulating cell stiffness, but it is not effective in gSC cells.

4. Discussion

In this study, we show that TRPV4 activity modulates SC cell mechanobiology, including cytoskeleton architecture, ECM protein expression/deposition, cell stiffness, and transcellular pore formation. In particular, we observe that human SC cells sense their substrate

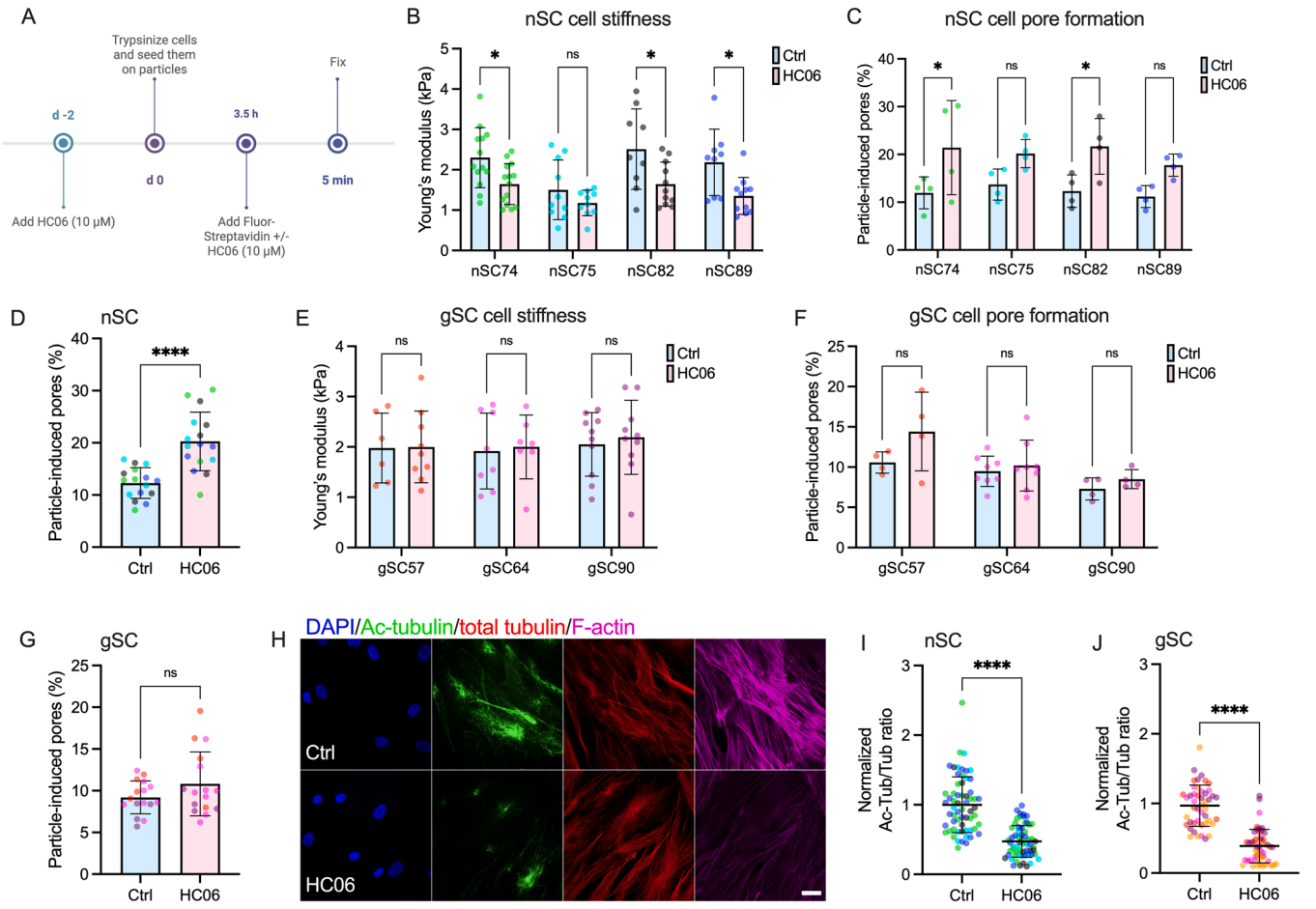


Fig. 6. Impact of prolonged TRPV4 inhibition on stiffness, transcellular pore formation, and MTs in SC cells. (A) Schematic illustrating the pore formation assay timeline: SC cells were treated with 10 μM HC06 in media containing 10 % FBS for 2 days, followed by trypsinization and plating on particles to induce pore formation. Cells were allowed to spread for 3.5 h under either control (DMSO) conditions, or with the TRPV4 antagonist HC06 (10 μM) added to the media, and transcellular pore formation was detected using fluorescently-tagged streptavidin. Created with BioRender.com. **(B, E)** Young's modulus of nSC and gSC cells measured by AFM (nSC cell: $n = 9$–14 cells per group; gSC cell: $n = 6$–10 cells per group). **(C, F)** Pore formation rate (percentage of particles with an associated pore) induced by particles in nSC ($n = 4$ wells per group) and gSC cells ($n = 4$–8 wells per group). **(D, G)** Pooled data on transcellular pore formation rate from all nSC and gSC cell strains. Symbols with different colors represent different cell strains. **(H)** Representative fluorescence micrographs of F-actin, acetylated α-tubulin (Ac-tubulin), and total α-tubulin in nSC cells treated with DMSO or TRPV4 antagonist HC06 (10 μM). Scale bar, 20 μm. **(I, J)** Ratio of acetylated to total microtubule fluorescent intensity in normal and gaucomatous SC cells ($n = 20$ images per group from 3 nSC/gSC cell strains with three replicates per cell strain). Symbols with different colors represent different cell strains. The lines and error bars indicate Mean ± SD. Significance was determined by two-way ANOVA using multiple comparisons tests (*$p < 0.05$, ****$p < 0.0001$).

stiffness, and that this interaction is modulated at least in part by TRPV4 activity (Fig. 7). Our data support the notion that acute TRPV4 activation induces Ca^{2+} influx, increasing transcellular pore formation in SC cells to facilitate outflow and decrease IOP in normal SC cells. Paradoxically, sustained TRPV4 inhibition in normal SC cells also increases transcellular pore formation. The situation in glaucomatous SC cells is slightly different: there are lower transcript levels of TRPV4, and the effects of TRPV4 activation and inhibition are attenuated as compared to the situation in normal SC cells.

In glaucoma, we postulate that impaired TRPV4 function in SC cells makes cells unable to counteract acute IOP transients, leading to sustained IOP elevation. Long-term IOP elevation induces stiffening of the SC inner wall cell substrate and TRPV4 activation, resulting in SC cell cytoskeletal and ECM remodeling. This causes SC cell stiffening, in turn reducing their transcellular pore formation ability, and creates a positive feedback loop that further increases IOP (Fig. 7).

A recent study identified an association between human genetic risk variants in mechanosensitive channels, such as TRPV4, and glaucoma [68]. Additionally, TRPV4 channels have been shown to influence IOP and conventional outflow facility in both mice [32,38,39] and *in vitro* studies, where trabecular meshwork cells were cultured on porous SU-8 polymers, by modulating trabecular meshwork cell function [32]. Our data demonstrated that TRPV4 activity also influences the mechanobiology of human SC cells in the outflow tract. Specifically, sustained inhibition of TRPV4 activity decreased F-actin and αSMA levels and the expression/deposition of ECM proteins (e.g., fibronectin, collagen types I and IV), which could be reversed by prolonged withdrawal of the TRPV4 inhibitor or by subsequent TRPV4 activation. αSMA, fibronectin, and collagen type I are markers of endothelial-to-mesenchymal transition (EndMT) [42,69,70], suggesting that sustained TRPV4 inhibition has the potential to block the EndMT of SC cells, thereby inhibiting cell pathology. Together with prior studies highlighting the role of TRPV4 in the trabecular meshwork, these results emphasize the importance of considering dysfunction in both the trabecular meshwork and SC when investigating the pathophysiology of ocular hypertension and developing therapeutic strategies to reduce outflow resistance.

The SC inner wall experiences a basal-to-apical pressure gradient which deforms SC cells to create giant vacuoles and transcellular pores that facilitate fluid drainage from the eye [10]. Our lab has previously developed an *in vitro* platform that utilizes micron-sized particles to

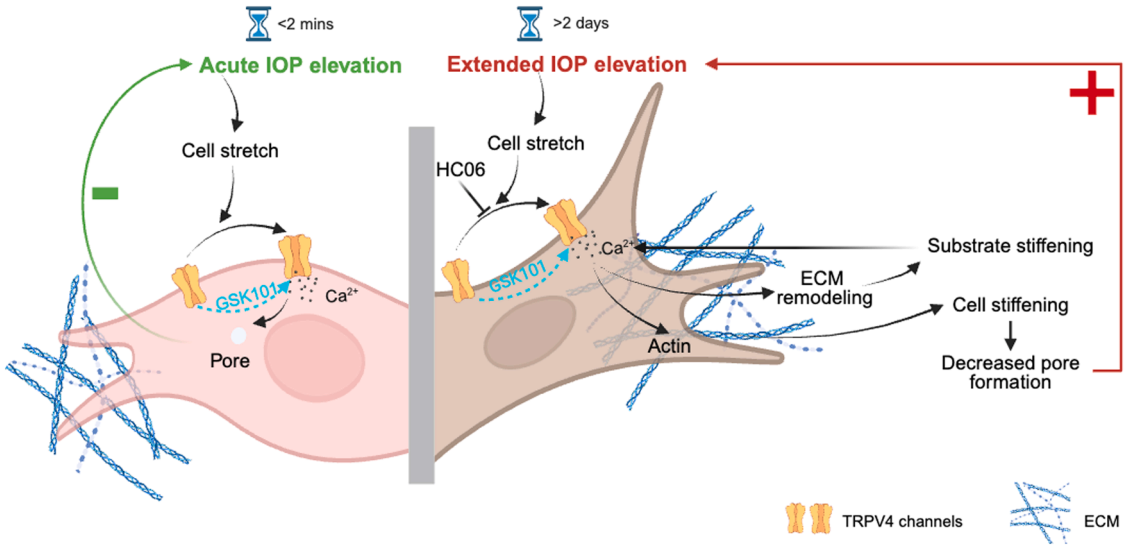


Fig. 7. Schematic for hypothesized role of TRPV4 mechanotransduction in SC cells. Under normal circumstances (left), acute IOP elevation activates TRPV4 channels, inducing Ca^{2+} influx and transcellular pore formation to facilitate aqueous outflow, thereby decreasing IOP and maintaining homeostasis. However, if IOP is chronically elevated (right), the SC inner wall cell substrate stiffens which induces elevation of intracellular Ca^{2+}, this leads to actin and ECM remodeling, increasing cell stiffness and forming a positive feedback loop that mitigates against IOP homeostasis. Sustained TRPV4 modulation influences SC cell mechanobiology, where inhibition reduces stiffness and increases transcellular pore formation, while activation has the opposite effect. The effects of TRPV4 modualtion are diminished in glaucomatous SC cells. Created with BioRender.com.

mimic the giant vacuoles and to apply basal-to-apical local cellular stretch, demonstrating the associated formation of transcellular pores in SC cells. Importantly, using this assay, we observed that the ability of SC cells to form pores significantly associated with cell stiffness [48]. In this study, we extended these findings to determine that prolonged TRPV4 inhibition led to SC cell softening and increased transcellular pore formation in SC cells. Although some variability in response was observed among different cell strains, potentially due to inherent cellular differences in sensitivity to dosage or treatment duration, the overall trend supports the potential of sustained TRPV4 inhibition to enhance outflow facility. Our findings indicate that TRPV4 activity modulates both F-actin organization and microtubule stability, two cytoskeletal systems likely involved in transcellular pore formation in SC cells. Both F-actin and microtubules may affect transcellular pore formation by modulating intracellular force generation and transmission, thereby facilitating coordinated fusion between the basal and apical membranes or between the plasma membrane and intracellular vesicular compartments [71,72]. Meanwhile, microtubule stability plays a critical role in supporting vesicular trafficking [73], which likely facilitates the membrane remodeling and fusion required for transcellular pore formation. Further studies are needed to define the specific contributions of F-actin and microtubule dynamics to this process, and to determine how these elements are integrated with TRPV4-mediated signaling – for example, by directly measuring membrane tension and cell traction forces that may influence transcellular pore formation.

Changes in the mechanical properties of the SC inner wall substrate have been implicated in the initiation and progression of glaucoma. For example, the substrate of the SC inner wall, known as the trabecular meshwork, is markedly stiffer in glaucoma [13,16,18]. To model this situation, we fabricated biomimetic hydrogel systems with stiffnesses mimicking the situation in normal and glaucomatous eyes. We observed that SC cells exhibited a higher level of intracellular Ca^{2+}, F-actin fibers, and cell stiffness on stiff substrates vs. on soft substrates, consistent with previous studies [51]. These studies thus identify TRPV4 channels as a modulator, and perhaps even a direct mechanosensor, of substrate stiffness sensing in SC cells. Further, on soft substrates, sustained TRPV4 activation increased SC cell stiffness, while conversely, TRPV4 inhibition reversed the cell stiffening induced by stiff substrates. While the data clearly implicate TRPV4 as a modulator of calcium levels and cell phenotype in response to matrix stiffness, other glaucoma-related mechanotransduction pathways, such as the YAP/TAZ signaling pathway [21,42], and other mechanosensitive channels, including PIEZO, TRPV2, and TRPM3 [68], may also play a role in the mechanotransduction in SC cells.

IOP can fluctuate within seconds due to physiological events like blinking and gaze adjustment [56,57]. Increased IOP causes stretching of the SC inner wall cell plasma membranes and thus very likely activates TRPV4. Previous studies have reported that acute cellular stretch (i.e., 2 min) induces transcellular pore formation in SC cells, which can be blocked by depleting endoplasmic reticulum or extracellular calcium [74,75]. Our data revealed that acute TRPV4 activation increased particle-induced pore formation in normal SC cells, which was blocked by co-treatment of TRPV4 antagonist with an agonist. Interestingly, we observed that treatment with the TRPV4 antagonist alone had no significant effect on transcellular pore formation. Several factors may explain this observation: (i) the experimental sequence, in which mechanical stretch from particles was applied before antagonist treatment, may have activated TRPV4 channels and triggered Ca^{2+} influx prior to inhibition; thus the antagonist may not have reversed early Ca^{2+} signaling events within the short experimental timeframe; (ii) compensatory activity from other mechanosensitive ion channels, such as PIEZO channels, could mask the effect of TRPV4 inhibition; and (iii) mechanical stretch may have induced internalization of TRPV4 channels [76], reducing their membrane localization and thereby limiting the efficacy of the antagonist. Topical administration of a TRPV4 agonist has been shown to lower nocturnal IOP in mouse eyes within 30 min of application [38]. We thus suggest that the rapid decrease in IOP following TRPV4 activation may be attributed to enhanced transcellular pore formation in the inner wall of SC.

Interestingly, our studies revealed that both TRPV4 activation and inhibition effects in SC cells derived from glaucomatous patients were diminished compared to observations in normal cells, as evidenced by smaller/no changes in cell stiffness and transcellular pore formation due to perturbation in TRPV4 activity. The normal and glaucomatous SC cell donors in this study were not age-matched, which is a common limitation in glaucoma research because glaucomatous donor eyes are typically obtained from older individuals. Thus, all glaucomatous SC cell strains in this study were derived from donors over 70 years of age,

however, three normal SC cell strains were also from relatively older donors (55–70 years). Notably, these age-comparable normal SC cells still exhibited stronger responses to TRPV4 modulation than did glaucomatous SC cells, suggesting that the reduced responsiveness seen in glaucomatous cells is associated with glaucoma rather than age per se. Testing this hypothesis will require further studies.

This diminished responsiveness in glaucomatous cells could be due to the decreased TRPV4 message levels and activity we observed in gSC cells. This loss of TRPV4 activity could impair the ability of SC inner wall cells to form transcellular pores in response to acute IOP elevations, compromising outflow function and IOP homeostasis. TRPV4 is known to internalize in response to agonist stimulation [76]. In glaucoma, persistently elevated IOP may lead to chronic TRPV4 activation, triggering its internalization and thereby reducing its functional activity. Preventing or reversing TRPV4 internalization might offer a therapeutic strategy to restore its function in SC cells. Potential approaches include modulating clathrin-mediated endocytosis [76] or post-translational modifications such as phosphorylation [77] to stabilize membrane-localized TRPV4. In addition, downstream signaling pathways of TRPV4, such as those involving calmodulin [78], protein kinase C (PKC) [79], and mitogen-activated protein kinase (MAPK) cascades [80], may contribute to the impaired transcellular pore formation observed in glaucomatous SC cells. Elucidating the specific contributions of these signaling mechanisms will require further investigation.

Our observations indicate that TRPV4 activation induces stiffening in normal SC cells. In contrast, gSC cells are inherently stiffer and exhibit lower TRPV4 activity compared to normal cells, suggesting additional factors influencing cell stiffness are altered in SC cells under glaucomatous conditions. The attenuated response to TRPV4 modulation observed in glaucomatous SC cells is likely reflective of impaired mechanotransduction signaling, potentially resulting from chronic exposure to elevated IOP. These observations highlight the complexity of SC cell mechanobiology in glaucoma, and therapeutic strategies targeting TRPV4 may need to be tailored to address these specific alterations.

TRPV4 is expressed across multiple ocular tissues, including the cornea, lens, ciliary body, trabecular meshwork, SC, and retina [29–35], where it contributes to essential physiological functions. Accordingly, therapeutic strategies targeting TRPV4 must account for the potential risk of off-target effects. To improve tissue specificity, it could be possible to use targeted delivery to SC. Such an approach has been achieved using self-assembled poly(ethylene glycol)-b-poly(propylene sulfide) (PEG-b-PPS) nanocarriers functionalized with an FLT4-specific peptide [81]. These nanocarriers selectively bind to VEGFR3, which is enriched on the inner wall of SC endothelial cells, enabling localized delivery of therapeutic agents. Such targeted approaches may enhance the safety and efficacy of TRPV4-based interventions.

5. Conclusion

This study demonstrates that TRPV4 plays a central role in modulating cytoskeleton organization, ECM remodeling, cell stiffness, substrate stiffness mechanotransduction, and transcellular pore formation in SC cells. TRPV4 modulation was markedly more effective in normal compared to glaucomatous SC cells. Specifically, treatment of normal SC cells cultured on stiff substrates with a TRPV4 antagonist significantly decreased cell stiffness and enhanced transcellular pore formation ability, thereby protecting normal cells from acquiring a glaucomatous SC-like phenotype. These results are in agreement with findings that TRPV4 knockout protects mouse eyes from developing high IOP [32,38]. Collectively, our data reveal that while TRPV4 has a key role in mechanotransduction in normal SC cells, this function seems to be impaired in glaucomatous SC cells. It is crucial to determine the timing and mechanism of the molecular changes in glaucomatous SC cells that impairs their response to TRPV4 activity modulation. Such insights will inform efforts to restore this function in glaucomatous SC cells and thus may guide future interventions in glaucoma pathology.

Data and materials availability

All data needed to evaluate the conclusions in the paper are present in the paper and/or the Supplementary Materials. Additional data related to this paper may be requested from the authors.

CRediT authorship contribution statement

Haiyan Li: Writing – review & editing, Writing – original draft, Methodology, Investigation, Conceptualization. **Cydney Wong:** Writing – review & editing, Methodology, Investigation. **Seyed Mohammad Siadat:** Writing – review & editing, Methodology. **Kristin M. Perkumas:** Writing – review & editing. **Jacques A. Bertrand:** Writing – review & editing, Methodology. **Darryl R. Overby:** Writing – review & editing, Methodology. **Todd Sulchek:** Writing – review & editing, Methodology. **W. Daniel Stamer:** Writing – review & editing, Methodology. **C. Ross Ethier:** Writing – review & editing, Writing – original draft, Supervision, Methodology, Investigation, Funding acquisition, Conceptualization.

Declaration of competing interest

The authors declare that they have no known competing financial interests or personal relationships that could have appeared to influence the work reported in this paper.

Acknowledgments

This study was financially supported Bright Focus Foundation: CG2020001 (CRE), G2024003F (HL); National Institutes of Health: 5R21EY033142-02 (CRE and DRO), R01EY028608 (WDS), R01EY022359 (WDS and DRO), T32 GM145735 (CAW), NIH Diversity Supplement EY031710-01S1 (CAW); BBSRC APP26196 (DRO); Georgia Research Alliance (CRE), and National Science Foundation Award Number 2134701 (TS) and CBET-2225476 (TS).

Supplementary materials

Supplementary material associated with this article can be found, in the online version, at doi:10.1016/j.actbio.2025.09.039.

References

[1] H.A. Quigley, Open-angle glaucoma, N. Engl. J. Med. 328 (15) (1993) 1097–1106.
[2] H.A. Quigley, A.T. Broman, The number of people with glaucoma worldwide in 2010 and 2020, Br. J. Ophthalmol. 90 (3) (2006) 262–267.
[3] E.R. Tamm, B.M. Braunger, R. Fuchshofer, Intraocular pressure and the mechanisms involved in resistance of the aqueous humor flow in the trabecular meshwork outflow pathways, Prog. Mol. Biol. Transl. Sci. 134 (2015) 301–314.
[4] R.F. Brubaker, Flow of aqueous humor in humans [the Friedenwald lecture], Invest. Ophthalmol. Vis. Sci. 32 (13) (1991) 3145–3166.
[5] N.E. Ashpole, D.R. Overby, C.R. Ethier, W.D. Stamer, Shear stress-triggered nitric oxide release from Schlemm's canal cells, Investig. Ophthalmol. Vis. Sci. 55 (12) (2014) 8067–8076.
[6] C.N. Dautriche, Y. Tian, Y. Xie, S.T. Sharfstein, A closer look at Schlemm's canal cell physiology: implications for biomimetics, J. Funct. Biomater. 6 (3) (2015) 963–985.
[7] W.D. Stamer, S.T. Braakman, E.H. Zhou, C.R. Ethier, J.J. Fredberg, D.R. Overby, M. Johnson, Biomechanics of Schlemm's canal endothelium and intraocular pressure reduction, Prog. Retin. Eye Res. 44 (2015) 86–98.
[8] C.R. Ethier, The inner wall of Schlemm's canal, Exp. Eye Res. 74 (2) (2002) 161–172.
[9] W.D. Stamer, B.C. Roberts, D.N. Howell, D.L. Epstein, Isolation, culture, and characterization of endothelial cells from Schlemm's canal, Invest. Ophthalmol. Vis. Sci. 39 (10) (1998) 1804–1812.
[10] A. HOLMBERG, The fine structure of the inner wall of Schlemm's canal, JAMA Arch. Ophthalmol. 62 (6) (1959) 956–958.
[11] R.R. Allingham, A.W. de Kater, C.R. Ethier, Schlemm's canal and primary open angle glaucoma: correlation between Schlemm's canal dimensions and outflow facility, Exp. Eye Res. 62 (1) (1996) 101–109.

[12] D.R. Overby, E.H. Zhou, R. Vargas-Pinto, R.M. Pedrigi, R. Fuchshofer, S. T. Braakman, R. Gupta, K.M. Perkumas, J.M. Sherwood, A. Vahabikashi, Q. Dang, J.H. Kim, C.R. Ethier, W.D. Stamer, J.J. Fredberg, M. Johnson, Altered mechanobiology of Schlemm's canal endothelial cells in glaucoma, Proc. Natl. Acad. Sci. U. S. A. 111 (38) (2014) 13876–13881.
[13] A. Vahabikashi, A. Gelman, B. Dong, L. Gong, E.D.K. Cha, M. Schimmel, E. R. Tamm, K. Perkumas, W.D. Stamer, C. Sun, H.F. Zhang, H. Gong, M. Johnson, Increased stiffness and flow resistance of the inner wall of Schlemm's canal in glaucomatous human eyes, Proc. Natl. Acad. Sci. 116 (52) (2019) 26555–26563.
[14] M. Johnson, D. Chan, A.T. Read, C. Christensen, A. Sit, C.R. Ethier, The pore density in the inner wall endothelium of Schlemm's canal of glaucomatous eyes, Invest. Ophthalmol. Vis. Sci. 43 (9) (2002) 2950–2955.
[15] R.R. Allingham, A.W. de Kater, C.R. Ethier, P.J. Anderson, E. Hertzmark, D. L. Epstein, The relationship between pore density and outflow facility in human eyes, Invest. Ophthalmol. Vis. Sci. 33 (5) (1992) 1661–1669.
[16] K. Wang, M.A. Johnstone, C. Xin, S. Song, S. Padilla, J.A. Vranka, T.S. Acott, K. Zhou, S.A. Schwaner, R.K. Wang, T. Sulchek, C.R. Ethier, Estimating Human trabecular meshwork stiffness by numerical modeling and advanced OCT imaging, Invest. Ophthalmol. Vis. Sci. 58 (11) (2017) 4809–4817.
[17] K. Wang, A.T. Read, T. Sulchek, C.R. Ethier, Trabecular meshwork stiffness in glaucoma, Exp. Eye Res. 158 (2017) 3–12.
[18] J.A. Last, T. Pan, Y. Ding, C.M. Reilly, K. Keller, T.S. Acott, M.P. Fautsch, C. J. Murphy, P. Russell, Elastic modulus determination of normal and glaucomatous Human trabecular meshwork, Invest. Ophthalmol. Vis. Sci. 52 (5) (2011) 2147–2152.
[19] H. Li, T. Bagué, A. Kirschner, A.N. Strat, H. Roberts, R.W. Weisenthal, A. E. Patteson, N. Annabi, W.D. Stamer, P.S. Ganapathy, S. Herberg, A tissue-engineered human trabecular meshwork hydrogel for advanced glaucoma disease modeling, Exp. Eye Res. 205 (2021) 108472.
[20] H. Li, V. Raghunathan, W.D. Stamer, P.S. Ganapathy, S. Herberg, Extracellular matrix stiffness and TGFβ2 regulate YAP/TAZ activity in Human trabecular meshwork cells, Front. Cell Dev. Biol. 10 (2022).
[21] H. Li, M. Kuhn, R.A. Kelly, A. Singh, K.K. Palanivel, I. Salama, M.L. De Ieso, W. D. Stamer, P.S. Ganapathy, S. Herberg, Targeting YAP/TAZ mechanosignaling to ameliorate stiffness-induced Schlemm's canal cell pathobiology, Am. J. Physiol. Cell Physiol. 326 (2) (2024) C513–C528.
[22] J. Árnadóttir, M. Chalfie, Eukaryotic mechanosensitive channels, Annu. Rev. Biophys. 39 (2010) 111–137. Volume 39, 2010.
[23] B. Martinac, Mechanosensitive ion channels: molecules of mechanotransduction, J. Cell. Sci. 117 (12) (2004) 2449–2460.
[24] B. Nilius, J. Vriens, J. Prenen, G. Droogmans, T. Voets, TRPV4 calcium entry channel: a paradigm for gating diversity, Am. J. Physiol. Cell Physiol. 286 (2) (2004) C195–C205.
[25] W. Everaerts, B. Nilius, G. Owsianik, The vanilloid transient receptor potential channel TRPV4: from structure to disease, Prog. Biophys. Mol. Biol. 103 (1) (2010) 2–17.
[26] S.O. Rahaman, L.M. Grove, S. Paruchuri, B.D. Southern, S. Abraham, K.A. Niese, R. G. Scheraga, S. Ghosh, C.K. Thodeti, D.X. Zhang, M.M. Moran, W.P. Schilling, D. J. Tschumperlin, M.A. Olman, TRPV4 mediates myofibroblast differentiation and pulmonary fibrosis in mice, J. Clin. Invest. 124 (12) (2014) 5225–5238.
[27] M. Zhang, Y. Ma, X. Ye, N. Zhang, L. Pan, B. Wang, TRP (transient receptor potential) ion channel family: structures, biological functions and therapeutic interventions for diseases, Signal. Transduct. Target. Ther. 8 (1) (2023) 261.
[28] B.D. Matthews, C.K. Thodeti, J.D. Tytell, A. Mammoto, D.R. Overby, D.E. Ingber, Ultra-rapid activation of TRPV4 ion channels by mechanical forces applied to cell surface beta1 integrins, Integr. Biol. (Camb) 2 (9) (2010) 435–442.
[29] Y. Okada, T. Sumioka, K. Ichikawa, H. Sano, A. Nambu, K. Kobayashi, K. Uchida, Y. Suzuki, M. Tominaga, P.S. Reinach, S.I. Hirai, J.V. Jester, M. Miyajima, K. Shirai, H. Iwanishi, W.W. Kao, C.Y. Liu, S. Saika, Sensory nerve supports epithelial stem cell function in healing of corneal epithelium in mice: the role of trigeminal nerve transient receptor potential vanilloid 4, Lab. Investig. 99 (2) (2019) 210–230.
[30] M. Shahidullah, A. Mandal, N.A. Delamere, A role for calcium-activated adenylate cyclase and protein kinase A in the lens src Family kinase and Na,K-ATPase response to hyposmotic stress, Invest. Ophthalmol. Vis. Sci. 58 (11) (2017) 4447–4456.
[31] M. Shahidullah, A. Mandal, N.A. Delamere, Damage to lens fiber cells causes TRPV4-dependent src family kinase activation in the epithelium, Exp. Eye Res. 140 (2015) 85–93.
[32] D.A. Ryskamp, A.M. Frye, T.T. Phuong, O. Yarishkin, A.O. Jo, Y. Xu, M. Lakk, A. Iuso, S.N. Redmon, B. Ambati, G. Hageman, G.D. Prestwich, K.Y. Torrejon, D. Križaj, TRPV4 regulates calcium homeostasis, cytoskeletal remodeling, conventional outflow and intraocular pressure in the mammalian eye, Sci. Rep. 6 (2016) 30583.
[33] M. Lakk, D. Križaj, TRPV4-Rho signaling drives cytoskeletal and focal adhesion remodeling in trabecular meshwork cells, Am. J. Physiol. Cell Physiol. 320 (6) (2021) C1013–c1030.
[34] H.A. Alkozi, M.J. Perez de Lara, J. Pintor, Melatonin synthesis in the human ciliary body triggered by TRPV4 activation: involvement of AANAT phosphorylation, Exp. Eye Res. 162 (2017) 1–8.
[35] T.J. Wubben, C.G. Besirli, D.N. Zacks, Pharmacotherapies for retinal detachment, Ophthalmology 123 (7) (2016) 1553–1562.
[36] N. Luo, M.D. Conwell, X. Chen, C.I. Kettenhofen, C.J. Westlake, L.B. Cantor, C. D. Wells, R.N. Weinreb, T.W. Corson, D.F. Spandau, K.M. Joos, C. Iomini, A. G. Obukhov, Y. Sun, Primary cilia signaling mediates intraocular pressure sensation, Proc. Natl. Acad. Sci. U. S. A. 111 (35) (2014) 12871–12876.
[37] T. Uchida, S. Shimizu, R. Yamagishi, S.M. Tokuoka, Y. Kita, R. Sakata, M. Honjo, M. Aihara, TRPV4 is activated by mechanical stimulation to induce prostaglandins release in trabecular meshwork, lowering intraocular pressure, PLoS One 16 (10) (2021) e0258911.
[38] S.N. Redmon, M. Lakk, Y.T. Tseng, C.N. Rudzitis, J.E. Searle, F. Ahmed, A. M. Unser, T. Borrás, K. Torrejon, D. Križaj, TRPV4 controls circadian and pathological ocular hypertension, J. Physiol. (2025).
[39] C.N. Rudzitis, M. Lakk, A. Singh, S.N. Redmon, D. Kirdajová, Y.-T. Tseng, M.L. De Ieso, W.D. Stamer, S. Herberg, D. Krizaj, TRPV4 activation by TGFβ2 enhances cellular contractility and drives ocular hypertension, Elife 14 (2025) RP104894.
[40] D.A. Ryskamp, P. Witkovsky, P. Barabas, W. Huang, C. Koehler, N.P. Akimov, S. H. Lee, S. Chauhan, W. Xing, R.C. Rentería, W. Liedtke, D. Krizaj, The polymodal ion channel transient receptor potential vanilloid 4 modulates calcium flux, spiking rate, and apoptosis of mouse retinal ganglion cells, J. Neurosci. 31 (19) (2011) 7089–7101.
[41] L. Taylor, K. Arnér, F. Ghosh, Specific inhibition of TRPV4 enhances retinal ganglion cell survival in adult porcine retinal explants, Exp. Eye Res. 154 (2017) 10–21.
[42] H. Li, A. Singh, K.M. Perkumas, W.D. Stamer, P.S. Ganapathy, S. Herberg, YAP/TAZ mediate TGFβ2-induced schlemm's canal cell dysfunction, Invest. Ophthalmol. Vis. Sci. 63 (12) (2022), 15-15.
[43] H. Li, J.L. Henty-Ridilla, A.M. Bernstein, P.S. Ganapathy, S. Herberg, TGFβ2 regulates human trabecular meshwork cell contractility via ERK and ROCK pathways with distinct signaling crosstalk dependent on the culture substrate, Curr. Eye Res. (2022) 1–41.
[44] A. Singh, R. Ghosh, H. Li, M.P. Geiss, H. Yoo, A.N. Strat, P.S. Ganapathy, S. Herberg, Three-dimensional extracellular matrix protein hydrogels for Human trabecular meshwork cell studies, in: T. Jakobs, P.B. Liton (Eds.), Glaucoma: Methods and Protocols, Springer US, New York, NY, 2025, pp. 17–29.
[45] H. Li, D.H. Harvey, J. Dai, S.P. Swingle, A.M. Compton, C.K. Sugali, K. Dhamodaran, J. Yao, T.-Y. Lin, T. Sulchek, T. Kim, C.R. Ethier, W. Mao, Characterization, enrichment, and computational modeling of cross-linked actin networks in transformed trabecular meshwork cells, Invest. Ophthalmol. Vis. Sci. 66 (2) (2025), 65-65.
[46] J. Schindelin, I. Arganda-Carreras, E. Frise, V. Kaynig, M. Longair, T. Pietzsch, S. Preibisch, C. Rueden, S. Saalfeld, B. Schmid, J.Y. Tinevez, D.J. White, V. Hartenstein, K. Eliceiri, P. Tomancak, A. Cardona, Fiji: an open-source platform for biological-image analysis, Nat. Methods 9 (7) (2012) 676–682.
[47] R. Vargas-Pinto, H. Gong, A. Vahabikashi, M. Johnson, The effect of the endothelial cell cortex on atomic force microscopy measurements, Biophys. J. 105 (2) (2013) 300–309.
[48] S.M. Siadat, H. Li, B.A. Millette, B.N. Safa, C.A. Wong, M.R.B. Fard, S.T. Braakman, I. Tay, J.A. Bertrand, A.T. Read, L.A. Schildmeyer, K.M. Perkumas, W.D. Stamer, D. R. Overby, C.R. Ethier, Endothelial cell stiffness and type drive the formation of biomechanically-induced transcellular pores, bioRxiv (2024), 2024.10.23.619950.
[49] C.A. Wong, N.S. Fraticelli Guzmán, A.T. Read, A. Hedberg-Buenz, M.G. Anderson, A.J. Feola, T. Sulchek, C.R. Ethier, A method for analyzing AFM force mapping data obtained from soft tissue cryosections, J. Biomech. 168 (2024) 112113.
[50] S.S. VanderWyst, K.M. Perkumas, A.T. Read, D.R. Overby, W.D. Stamer, Structural basement membrane components and corresponding integrins in Schlemm's canal endothelia, Mol. Vis. 17 (2011) 199–209.
[51] H. Li, M. Kuhn, R.A. Kelly, A. Singh, K.K. Palanivel, I. Salama, M.L.D. Ieso, W. D. Stamer, P.S. Ganapathy, S. Herberg, Targeting YAP mechanosignaling to ameliorate stiffness-induced Schlemm's canal cell pathobiology, bioRxiv (2023), 2023.09.08.556840.
[52] O. Dushek, S. Mueller, S. Soubies, D. Depoil, I. Caramalho, D. Coombs, S. Valitutti, Effects of intracellular calcium and actin cytoskeleton on TCR mobility measured by fluorescence recovery, PLoS One 3 (12) (2008) e3913.
[53] M. Yoneda, T. Nishizaki, K. Tasaka, H. Kurachi, A. Miyake, Y. Murata, Changes in actin network during calcium-induced exocytosis in permeabilized GH3 cells: calcium directly regulates F-actin disassembly, J. Endocrinol. 166 (3) (2000) 677–687.
[54] R.A. Kelly, K.M. Perkumas, M. Campbell, G.J. Farrar, W.D. Stamer, P. Humphries, J. O'Callaghan, C.J. O'Brien, Fibrotic changes to Schlemm's canal endothelial cells in glaucoma, Int. J. Mol. Sci. 22 (17) (2021).
[55] W.D. Stamer, A.F. Clark, The many faces of the trabecular meshwork cell, Exp. Eye Res. 158 (2017) 112–123.
[56] D.J. Coleman, S. Trokel, Direct-recorded intraocular pressure variations in a human subject, Arch. Ophthalmol. 82 (5) (1969) 637–640.
[57] J.E. Markert, J.V. Jasien, D.C. Turner, C. Huisingh, C.A. Girkin, J.C. Downs, IOP transient impulse, ocular perfusion pressure, and mean arterial pressure relationships in nonhuman primates instrumented with telemetry, Invest. Ophthalmol. Vis. Sci. 59 (11) (2018) 4496–4505.
[58] J.C. Hay, Calcium: a fundamental regulator of intracellular membrane fusion? EMBo Rep. 8 (3) (2007) 236–240.
[59] S.M. Siadat, J.A. Bertrand, D.R. Overby, W.D. Stamer, C.R. Ethier, Development of a Schlemm's canal "Inner Wall on a Chip" for high content screening, Invest. Ophthalmol. Vis. Sci. 64 (8) (2023) 50. -50.
[60] A. Vahabikashi, S.A. Adam, O. Medalia, R.D. Goldman, Nuclear lamins: structure and function in mechanobiology, APL Bioeng. 6 (1) (2022) 011503.
[61] D. Wen, Y. Gao, Y. Liu, C. Ho, J. Sun, L. Huang, Y. Liu, Q. Li, Y. Zhang, Matrix stiffness-induced α-tubulin acetylation is required for skin fibrosis formation through activation of Yes-associated protein, MedComm (2020) 4 (4) (2023) e319.
[62] S. Seetharaman, B. Vianay, V. Roca, A.J. Farrugia, C. De Pascalis, B. Boëda, F. Dingli, D. Loew, S. Vassilopoulos, A. Bershadsky, M. Théry, S. Etienne-

Manneville, Microtubules tune mechanosensitive cell responses, Nat. Mater. 21 (3) (2022) 366–377.
[63] A.K. Coleman, H.C. Joca, G. Shi, W.J. Lederer, C.W. Ward, Tubulin acetylation increases cytoskeletal stiffness to regulate mechanotransduction in striated muscle, J. Gen. Physiol. 153 (7) (2021).
[64] S. Gu, Y. Liu, B. Zhu, K. Ding, T.P. Yao, F. Chen, L. Zhan, P. Xu, M. Ehrlich, T. Liang, X. Lin, X.H. Feng, Loss of α-tubulin acetylation is associated with TGF-β-induced epithelial-mesenchymal transition, J. Biol. Chem. 291 (10) (2016) 5396–5405.
[65] C.L. Marchant, A.N. Malmi-Kakkada, J.A. Espina, E.H. Barriga, Cell clusters softening triggers collective cell migration *in vivo*, Nat. Mater. 21 (11) (2022) 1314–1323.
[66] J.N. Heck, S.M. Ponik, M.G. Garcia-Mendoza, C.A. Pehlke, D.R. Inman, K. W. Eliceiri, P.J. Keely, Microtubules regulate GEF-H1 in response to extracellular matrix stiffness, Mol. Biol. Cell 23 (13) (2012) 2583–2592.
[67] Z. Xu, L. Schaedel, D. Portran, A. Aguilar, J. Gaillard, M.P. Marinkovich, M. Théry, M.V. Nachury, Microtubules acquire resistance from mechanical breakage through intralumenal acetylation, Science (1979) 356 (6335) (2017) 328–332.
[68] W.W. Liu, T.G. Kinzy, J.N. Cooke Bailey, Z. Xu, P. Hysi, J.L. Wiggs, R.R. Allingham, M. Brilliant, D.L. Budenz, J.H. Fingert, D. Gaasterland, T. Gaasterland, J.L. Haines, M.A. Hauser, R.K. Lee, P.R. Lichter, Y. Liu, S. Moroi, J. Myers, L.R. Pasquale, M. Pericak-Vance, A. Realini, D. Rhee, J.E. Richards, R. Ritch, J.S. Schuman, W. K. Scott, K. Singh, A.J. Sit, D. Vollrath, R.N. Weinreb, G. Wollstein, D.J. Zack, N. Consortium, Mechanosensitive ion channel gene survey suggests potential roles in primary open angle glaucoma, Sci. Rep. 13 (1) (2023) 15871.
[69] K.J. Choi, J.-K. Nam, J.-H. Kim, S.-H. Choi, Y.-J. Lee, Endothelial-to-mesenchymal transition in anticancer therapy and normal tissue damage, Exp. Mol. Med. 52 (5) (2020) 781–792.
[70] J. Ma, G. Sanchez-Duffhues, M.-J. Goumans, P. ten Dijke, TGF-β-induced endothelial to mesenchymal transition in disease and tissue engineering, Front. Cell Dev. Biol. 8 (2020).
[71] J.H. Kim, Y. Ren, W.P. Ng, S. Li, S. Son, Y.S. Kee, S. Zhang, G. Zhang, D.A. Fletcher, D.N. Robinson, E.H. Chen, Mechanical tension drives cell membrane fusion, Dev. Cell 32 (5) (2015) 561–573.
[72] G.M. Sumida, S. Yamada, Self-contact elimination by membrane fusion, Proc. Natl. Acad. Sci. 110 (47) (2013) 18958–18963.
[73] J. Qu, J. Li, H. Wang, J. Lan, Z. Huo, X. Li, Decoding the role of microtubules: a trafficking road for vesicle, Theranostics 15 (11) (2025) 5138–5152.
[74] J.A. Bertrand, C.R. Ethier, W.D. Stamer, D.R. Overby, Extracellular calcium entry via mechanosensitive ion channels is necessary for transcellular pore formation in Schlemm's canal endothelial cells, Invest. Ophthalmol. Vis. Sci. 65 (7) (2024) 5155. -5155.
[75] J.A. Bertrand, W.D. Stamer, D.R. Overby, Mapping the stretch dependence of pore formation in normal versus glaucomatous Schlemm's canal cells, Invest. Ophthalmol. Vis. Sci. 64 (8) (2023) 5079. -5079.
[76] S. Baratchi, P. Keov, W.G. Darby, A. Lai, K. Khoshmanesh, P. Thurgood, P. Vahidi, K. Ejendal, P. McIntyre, The TRPV4 agonist GSK1016790A regulates the membrane expression of TRPV4 channels, Front. Pharmacol. 10 (2019) 6.
[77] H.C. Fan, X. Zhang, P.A. McNaughton, Activation of the TRPV4 ion channel is enhanced by phosphorylation, J. Biol. Chem. 284 (41) (2009) 27884–27891.
[78] R. Masuyama, A. Mizuno, H. Komori, H. Kajiya, A. Uekawa, H. Kitaura, K. Okabe, K. Ohyama, T. Komori, Calcium/calmodulin-signaling supports TRPV4 activation in osteoclasts and regulates bone mass, J. Bone Miner. Res. 27 (8) (2012) 1708–1721.
[79] R.K. Adapala, P.K. Talasila, I.N. Bratz, D.X. Zhang, M. Suzuki, J.G. Meszaros, C. K. Thodeti, PKCα mediates acetylcholine-induced activation of TRPV4-dependent calcium influx in endothelial cells, Am. J. Physiol. Heart. Circ. Physiol. 301 (3) (2011) H757–H765.
[80] P. Jie, Z. Hong, Y. Tian, Y. Li, L. Lin, L. Zhou, Y. Du, L. Chen, L. Chen, Activation of transient receptor potential vanilloid 4 induces apoptosis in hippocampus through downregulating PI3K/Akt and upregulating p38 MAPK signaling pathways, Cell Death. Dis. 6 (6) (2015) e1775. -e1775.
[81] T. Stack, M. Vincent, A. Vahabikashi, G. Li, K.M. Perkumas, W.D. Stamer, M. Johnson, E. Scott, Targeted delivery of cell softening micelles to Schlemm's canal endothelial cells for treatment of glaucoma, Small. 16 (43) (2020) e2004205.